Research Square

Preprints are preliminary reports that have not undergone peer review.
They should not be considered conclusive, used to inform clinical practice,
or referenced by the media as validated information.

Diagnostic and Prognostic Value of Cerebrospinal Fluid Biomarkers in Lung Cancer Brain Metastasis: A Proteomic Analysis

Yinuo Jin
the Second Affiliated Hospital of Dalian Medical University
Yang Xu
the Second Affiliated Hospital of Dalian Medical University
Wenwen Liu
the Second Affiliated Hospital of Dalian Medical University
Mingliang Ye
National Chromatographic R&A Center, Chinese Academy of Sciences (CAS)
Song Wei
Capital Medical University
Xin You
the Second Affiliated Hospital of Dalian Medical University
Qi Wang
wqdlmu@163.com

the Second Affiliated Hospital of Dalian Medical University

Research Article

Keywords: lung cancer brain metastasis (LCBM), cerebrospinal fluid (CSF), proteomics, biomarker, prognosis

Posted Date: November 13th, 2026

DOI: https://doi.org/10.21203/rs.3.rs-11521327/v1

License: This work is licensed under a Creative Commons Attribution 4.0 International License.
Read Full License

Additional Declarations: No competing interests reported.

Diagnostic and Prognostic Value of Cerebrospinal Fluid Biomarkers in Lung Cancer Brain Metastasis: A Proteomic Analysis

Yinuo Jin[1#], Yang Xu[1#], Wenwen Liu[2], Mingliang Ye[3,4], Song Wei[5], Xin You[*2], Qi Wang[*1,2]

1 Department of Respiratory Medicine, the Second Affiliated Hospital of Dalian Medical University, Dalian, China, 116023

2 Lung Cancer Transitional Medicine Center, The Second Affiliated Hospital of Dalian Medical University, Dalian, China, 116023

3 State Key Laboratory of Medical Proteomics, CAS Key Laboratory of Separation Sciences for Analytical Chemistry, National Chromatographic R&A Center, Dalian Institute of Chemical Physics, Chinese Academy of Sciences (CAS), Dalian, China.

4 University of Chinese Academy of Sciences, Beijing, China.

5 Department of Pulmonary Oncology, Beijing Chest Hospital, Capital Medical University, Beijing, China, 101149

#These authors contributed equally to this work.

*Corresponding authors: Professor Xin You (alchemist_riot@126.com) and Professor Qi Wang (wqdlmu@163.com), The Second Affiliated Hospital of Dalian Medical University, Dalian, China, 116023

Abstract

Background: Lung cancer brain metastasis (LCBM) is a severe complication with a poor prognosis, and reliable cerebrospinal fluid (CSF) biomarkers for its diagnosis are lacking. We aimed to discover and validate CSF protein markers that may aid the differential diagnosis of LCBM against common neurological conditions and to explore their diagnostic and prognostic value. **Methods:** In a discovery cohort (n = 56) of LCBM patients and non-tumor controls undergoing lumbar puncture, high-precision proteomic mass spectrometry with permutation-based false discovery rate control screened differentially expressed proteins (DEPs). Candidate DEPs were validated by ELISA in a validation cohort (n = 78) comprising LCBM patients and disease controls with primary intracranial tumors, CNS lymphoma, encephalitis, cerebral hemorrhage, or epilepsy. Diagnostic performance was assessed by receiver operating characteristic analysis, with bootstrap validation and calibration of combined models.

Prognosis was evaluated by Kaplan–Meier analysis (log-rank p adjusted for data-driven cutoff selection), Cox regression, and formal comparison of discriminative ability (C-index, time-dependent AUC, likelihood-ratio tests). **Results:** ELISA confirmed differential expression of the candidates. KLK6 showed near-perfect discrimination of LCBM from all disease-control subgroups (AUC = 0.969), whereas sFRP4 and FBLN1 showed moderate accuracy. A combined model incorporating KLK6 achieved an AUC of 0.989 (95% CI, 0.976–1.000), and sFRP4 + FBLN1 yielded 0.797 (95% CI, 0.697–0.897; bootstrap-corrected 0.791). Higher CSF POSTN was associated with shorter overall survival (median, 19.0 vs. 51.0 months; HR = 2.05 per SD, 95% CI 1.25–3.37, p = 0.005), which persisted after adjustment for age (HR = 1.74 per SD, 95% CI 1.10–2.77, p = 0.019) and targeted therapy (HR = 0.56, 0.25–1.26, p = 0.163). Discrimination was higher for CSF POSTN than for CSF CEA (C-index, 0.749 vs. 0.577; difference, 0.171; 95% CI 0.016–0.303), although 36-month time-dependent AUC did not differ significantly; no superiority over CEA is claimed. **Conclusion:** Integrating proteomics and immunoassays identified candidate CSF biomarkers differentiating LCBM from a spectrum of non-malignant and malignant neurological diseases. Because no NSCLC control group without brain metastasis was included, LCBM specificity has not been established; these markers should be regarded as preliminary auxiliary tools requiring independent external validation.

Keywords: lung cancer brain metastasis (LCBM); cerebrospinal fluid (CSF); proteomics; biomarker; prognosis

Introduction

Lung cancer remains one of the most prevalent and lethal malignancies globally, representing the leading cause of cancer-related mortality[1]. Non-small cell lung cancer (NSCLC) accounts for approximately 85% of all lung cancer cases[2], predominantly consisting of lung adenocarcinoma (LUAD) and lung squamous cell carcinoma (LUSC). The prognosis for patients with advanced (Stage III) and metastatic (Stage IV) NSCLC remains dismal, with 5-year survival rates of approximately 15% and 5%, respectively[3]. The brain is the most frequent site of distant metastasis in lung cancer[4]. Due to the impermeability of the blood-brain barrier (BBB), the central nervous system (CNS) frequently acts as a "sanctuary site," shielding tumor cells from systemic therapies[5]. Despite advances in local and systemic treatments—including targeted therapy, radiotherapy, and chemotherapy—which have improved outcomes, the prognosis for patients with lung cancer brain metastasis (LCBM) remains poor, with a median overall survival of only 4 to 9 months after the diagnosis of brain metastasis[6]. Early detection and timely therapeutic intervention are therefore critical for optimizing clinical management and improving survival.

At present, the diagnosis of brain parenchymal metastases from lung cancer relies primarily on neuroimaging, particularly contrast-enhanced magnetic resonance imaging (MRI)[8]. Although MRI is highly sensitive for established metastases, its performance is limited for micrometastatic disease, and it cannot reliably distinguish true tumor progression from treatment-related changes such as radiation necrosis. Cerebrospinal fluid (CSF) cytology obtained by lumbar puncture is highly specific, principally for leptomeningeal disease[9], but its sensitivity is low in parenchymal metastasis and repeated invasive procedures are required. There is thus an urgent need for CSF-derived biomarkers that can be obtained at a single, diagnostically indicated lumbar puncture to complement neuroimaging, improve diagnostic accuracy and enable dynamic monitoring of disease course.

Liquid biopsy has emerged as a promising tool in oncology, offering unique insights into the tumor microenvironment**Error! Reference source not found.**. CSF is a particularly informative source of molecular biomarkers: because it is in direct contact with the CNS tumor microenvironment and can be regarded as an extension of the CNS interstitial space, it acts as a reservoir reflecting the pathophysiological state of brain tumors[10]. Tumor-derived analytes are considerably more abundant in CSF than in plasma, particularly in the setting of leptomeningeal metastasis[12], providing a minimally invasive alternative to surgical biopsy for diagnosis and treatment monitoring[13]. Within this framework, proteomics is well positioned to extend the reach of precision oncology by capturing dynamic, patient-specific protein networks[14][15] , and proteomic profiling of CSF therefore offers a powerful strategy for discovering biomarkers that reflect the pathophysiology of brain metastasis.

Nevertheless, original studies of CSF biomarkers in patients with brain metastasis remain scarce. In a mass-spectrometric analysis of 251 CSF samples spanning four brain malignancy types, Schmid et al. demonstrated that CSF proteome deregulation arises largely from blood–brain barrier disruption and is broadly conserved across brain tumor entities[16] — a framework against which any candidate CSF marker must be interpreted. In parallel, analyses of CSF cell-free tumor DNA have shown that the CSF compartment reflects the genomic alterations of brain tumors more faithfully than plasma[17]. In our own previous work, CTSF and FBLN1 were identified as diagnostic CSF biomarkers for brain metastasis of NSCLC[18]. Building on that study, the present work adds KLK6 and sFRP4 as new candidate markers, provides the first prognostic evaluation of CSF POSTN, and uses neurological disease controls rather than non-neurological controls, thereby testing the candidates against the genuine clinical differential diagnosis of LCBM.

In this study, we therefore applied an integrated two-cohort design that combined discovery-phase proteomic screening with immunoassay validation to identify differentially expressed CSF proteins, with the aim of deriving candidate biomarkers capable of distinguishing LCBM from the common non-malignant and malignant neurological conditions encountered in its differential diagnosis. We subsequently evaluated the diagnostic performance of these candidates, together with internal validation of the combined models, and their association with overall survival. Our findings extend our previous work by adding new candidate markers and providing a first prognostic assessment of the CSF molecular landscape of LCBM, thereby highlighting promising auxiliary biomarkers for diagnosis and prognostic stratification that warrant confirmation in independent cohorts (Figure 1).

Results

Screening of Target Proteins via CSF Proteomics in the Discovery Cohort

Baseline Characteristics and Proteomic Profiling

A total of 56 subjects were enrolled in the discovery cohort, comprising 28 patients with brain metastases from NSCLC (hereafter referred to as the LCBM group) and 28 controls who underwent lumbar puncture for spinal anesthesia during joint surgery. As detailed in Table 1, the distribution of sex was comparable between the LCBM and control groups ($\chi^2 = 0.686$, $p = 0.408$), whereas the control group was significantly older than the LCBM group (65.64 ± 8.01 vs. 58.89 ± 7.31 years, $p = 0.002$). This age difference is attributable to the composition of the control cohort, which consisted of predominantly middle-aged and elderly individuals undergoing orthopedic joint surgery, whereas patients with LCBM were relatively younger at enrollment. Because the control group was significantly older, we additionally performed an age-adjusted sensitivity analysis of the entire screen (analysis of covariance with age as a covariate for each protein): 851 of the 855 proteins reported as significant at $p < 0.01$ were reproduced in this re-analysis, and 824 of these (96.8%) remained significant after adjustment for age ($p < 0.05$); 99% of the FDR-significant proteins ($q < 0.01$) likewise remained significant, and all nine validated candidates belonged to this set; of these, the four with the strongest statistical evidence (CTSF, MSLN, KLK6 and LCN2) retained age-adjusted $p < 0.01$ (Supplementary Table 1). The proteomic differences reported below are therefore not explained by the age imbalance. Of the 56 samples in the discovery cohort, 28 LCBM samples comprised 23 from Beijing Chest Hospital, Capital Medical University and 5 from The Second Hospital of Dalian Medical University, and all 28 control samples were from The Second Hospital of Dalian Medical University (Supplementary Table 2A).

Global CSF proteomic profiling

High-resolution mass spectrometry identified a total of 1,674 proteins in the CSF samples from the discovery cohort. Comparative analysis revealed distinct expression patterns between the two groups (Figure 2A): compared with the control group, 314 proteins were significantly upregulated and 420 were significantly downregulated in the LCBM group (volcano-plot criteria: $p < 0.05$ and $|\text{difference in mean log2 intensity}| \geq 1$, equivalent to at least a 2-fold change in either direction). Exact p and q values for all 1,674 quantified proteins are provided in Supplementary Table 3. A more stringent two-step filter ($p < 0.01$ and $q < 0.01$) was applied for the subsequent pathway enrichment and candidate selection (Supplementary Table 3A). Principal component analysis (PCA) demonstrated a distinct separation between the LCBM and control clusters based on their global proteomic profiles (Figure 2B), and heatmap visualization illustrated the distinct expression profiles of differentially expressed proteins (DEPs) between the groups (Figure 2C).

Functional Enrichment Analysis

To elucidate the biological implications of the observed proteomic changes, Gene Ontology (GO) and Kyoto Encyclopedia of Genes and Genomes (KEGG) enrichment analyses were performed on the DEPs. GO analysis indicated that upregulated proteins were primarily enriched in cellular components the extracellular region and nucleosome, and biological processes involving immune response and chromatin organization (Figure 2D – E). Downregulated proteins were largely associated with synaptic structures and nervous system development. KEGG pathway analysis revealed that upregulated proteins were significantly involved in systemic lupus erythematosus, proteasome function, and neutrophil extracellular trap formation, while downregulated proteins were linked to cell adhesion molecule (CAM) interaction and axon guidance (Figure 2G – H). Consistent with previous studies, these enrichment patterns are compatible with alterations in the tumor microenvironment and neuro-immune interactions in patients with LCBM; we note, however, that enrichment analysis reflects functional annotation of differentially abundant proteins and does not constitute a direct measurement of immune activity in our cohort[19]. Tumor-related KEGG pathways were then used to define the candidate pools for biomarker selection (Supplementary Figure 1).

Selection of Candidate Biomarkers

To ensure a transparent and reproducible selection process, a stepwise screening workflow with predefined criteria was applied to the 1,674 quantified proteins (Supplementary Figure 1). The candidate pool was defined by two sequential significance filters: nominal (unadjusted) statistical significance ($p < 0.01$; $n = 855$) and permutation-based multiple-testing significance ($q < 0.01$; $n = 553$, comprising 234 upregulated and 319 downregulated proteins). The volcano-plot effect-size threshold (|difference in mean log2 intensity| $\geqslant$ 1, i.e. $\geqslant$ 2-fold; $n = 734$ at $p < 0.05$ and $n = 680$ at $p < 0.01$) is given for every quantified protein in Supplementary Table 3 and defines the differentially expressed proteins shown in Figure 2A, but was not used as an inclusion criterion: in a 56-sample CSF cohort, effect sizes are attenuated by pre-analytical variability and compartment heterogeneity, so the pool was defined by significance alone. All nine proteins subsequently selected met this threshold (1.02–3.00 log2, i.e. 2.03–8.00-fold). KEGG enrichment analysis of the pool identified 8 tumor-related pathways (90 proteins) among the upregulated and 4 tumor-related pathways (55 proteins) among the downregulated proteins; 68 of the 90 upregulated and 54 of the 55 downregulated proteins were taken forward to detailed stepwise screening (Supplementary Tables 4 and 5). From these candidate pools, biomarkers were selected according to four predefined criteria: (i) statistical robustness, including both unadjusted significance and FDR-adjusted q values; (ii) biological plausibility, requiring a soluble, extracellularly detectable form and documented involvement in tumorigenesis, extracellular matrix remodeling, or metastatic colonization, with preference for changes reflecting tumor-specific biology rather than nonspecific neural injury; (iii) detectability in CSF, supported by quantification in our dataset and reported detection in cerebrospinal fluid; and (iv)

technical feasibility, namely the availability of commercial ELISA kits and precedent for validation in CSF matrix. The complete ranked protein lists with stepwise filtering decisions are provided in Supplementary Tables 4 (downregulated) and 5 (upregulated). Ultimately, nine candidate biomarkers were selected for validation in the subsequent large-sample cohort: cathepsin F (CTSF), mesothelin (MSLN), mucin-1 (MUC1), fibulin-1 (FBLN1), kallikrein-6 (KLK6), periostin (POSTN), CD166 antigen (ALCAM), neutrophil gelatinase-associated lipocalin (LCN2), and secreted frizzled-related protein 4 (sFRP4).

Validation of Candidate Biomarkers in the Independent Cohort

Baseline Characteristics of the Validation Cohort

To validate the candidate biomarkers identified in the discovery phase, an independent validation cohort comprising 78 subjects was enrolled. This cohort included 38 patients with LCBM and 40 disease controls. The LCBM group consisted of patients with adenocarcinoma (n = 38), including one case of adenosquamous carcinoma. The control group included a heterogeneous group of neurological disorders to ensure diagnostic specificity, including primary intracranial tumors (n = 11), lymphoma with CNS involvement (n = 5), encephalitis (n = 6), cerebral hemorrhage (n = 12), and epilepsy or other causes of impaired consciousness (n = 6; hereafter, the epilepsy subgroup). Demographic and clinical characteristics are summarized in Table 1B. Age did not differ significantly across the LCBM and control subgroups (one-way ANOVA across the six groups, p = 0.209), although the control group had a considerably wider age distribution (range 16–81 vs 36–77 years); gender was likewise comparable (p = 0.473). Detailed per-patient characteristics of the LCBM group are provided in Supplementary Table 2B; briefly, the 38 patients had a median age of 63.0 years (range 36–77), 37 had adenocarcinoma and 1 had adenosquamous carcinoma, and 27 (71.1%) harbored a driver gene alteration (EGFR mutation, n = 19 [50.0%]; ALK fusion, n = 3; KRAS mutation, n = 4; RET rearrangement, n = 1). With overall survival defined from the date of the initial lung cancer diagnosis (data cut-off, June 2026), the median overall survival was 30.5 months (range 11–110), with 32 deaths and 6 censored patients. Of the 78 samples, the 38 LCBM samples comprised 31 from Beijing Chest Hospital, Capital Medical University and 7 from The Second Hospital of Dalian Medical University, and all 40 control samples were from The Second Hospital of Dalian Medical University. All 68 control samples of the two cohorts were therefore recruited at a single center, whereas 54 of the 66 LCBM samples were recruited at the other center (Supplementary Tables 2 and 6).

Verification of Candidate Biomarkers via ELISA

The nine candidate proteins were then quantified by ELISA in the validation cohort. Figure 3A presents a heatmap of these proteins across the validation cohort, illustrating their differential expression patterns. ELISA quantification revealed no significant differences in CSF levels of

CTSF, MSLN, or MUC1 between the LCBM and control groups (p = 0.798, 0.242 and 0.960, respectively; Figure 3B, Table 2A), indicating their limited utility as specific diagnostic markers in this setting. In contrast, the remaining six proteins showed significant alterations (Figure 3C, D, Table 2A). POSTN, ALCAM, LCN2, and sFRP4 were significantly upregulated in the LCBM group ($p < 0.05$) For POSTN, however, this difference was small and was not reproduced within the single center that contributed both cases and controls (7 LCBM vs 40 controls: median 295.4 vs 340.7 ng/mL; AUC 0.450; p = 0.692), and POSTN showed only a borderline difference between centers among LCBM patients (median 295.4 vs 343.5 ng/mL; p = 0.073), so that a center-related contribution cannot be excluded (Supplementary Table 6); POSTN was therefore evaluated further only as a prognostic marker within LCBM. Conversely, FBLN1 and KLK6 were significantly downregulated in the LCBM group (both $p < 0.01$). Although FBLN1 concentrations exceeded those of KLK6 in absolute terms within the LCBM group, both proteins were markedly decreased relative to controls. Figure 3E summarizes the validated candidate biomarkers, categorized into upregulated (POSTN, ALCAM, LCN2, sFRP4) and downregulated (FBLN1, KLK6) groups. These findings suggest that a specific panel of CSF proteins is dysregulated in LCBM, supporting their potential utility as candidate auxiliary markers within the differential diagnosis of LCBM (see Limitations).

Diagnostic Performance of Biomarkers

Evaluation of Biomarkers Across Control Subgroups

To evaluate biomarker specificity, we analyzed the expression profiles of sFRP4, FBLN1, and KLK6 across specific control subgroups (Figure 4A, Table 2B). Post-hoc comparisons of the LCBM group with each control subgroup were performed using two-sided Mann–Whitney U tests for independent samples, and p values were adjusted for the five prespecified subgroup contrasts using the Holm–Bonferroni step-down procedure. CSF KLK6 showed the most pronounced and consistent intergroup separation: it was significantly lower in the LCBM group than in every control subgroup — primary intracranial tumors (median 1.43 vs. 2.31 ng/mL), lymphoma, encephalitis, cerebral hemorrhage, and epilepsy (all adjusted $p < 0.001$; exact adjusted p values in Supplementary Table 7) — as well as versus all controls combined (nominal $p < 0.001$). sFRP4 was significantly elevated in the LCBM group relative to all controls combined (nominal $p < 0.001$); after adjustment, this elevation remained significant against CNS lymphoma (adjusted p = 0.008), showed a borderline trend against primary intracranial tumors (adjusted p = 0.054), but did not survive correction against cerebral hemorrhage or epilepsy (both adjusted p = 0.086), and no difference was observed against encephalitis (adjusted p = 0.374). FBLN1 was lower in the LCBM group than in every control subgroup; the reduction was significant against cerebral haemorrhage (adjusted p = 0.009) and showed the same direction against CNS lymphoma and encephalitis (both adjusted p = 0.089), but was not significant against primary intracranial tumours or epilepsy (both adjusted p =

0.462). These findings indicate that KLK6 is the only candidate exhibiting consistent discriminatory performance across all control subgroups after multiple-testing correction, supporting its value for distinguishing LCBM from diverse neurological disorders within this case–control setting (Supplementary Table 8). Within the single center that contributed both cases and controls (7 Dalian LCBM vs 40 Dalian controls), the case–control differences of sFRP4 (AUC 0.846, p = 0.002) and FBLN1 (AUC 0.743, p = 0.042) were likewise reproduced, and neither protein differed between LCBM patients recruited at the two centers (p = 0.220 and p = 0.797, respectively), indicating that — as for KLK6 — these differences are not attributable to a center effect (Supplementary Table 6).

Diagnostic Efficacy of Individual Biomarkers

ROC curve analysis revealed that POSTN, ALCAM, and LCN2 had limited diagnostic value for LCBM (AUC 0.572–0.735), as their high sensitivity was consistently offset by modest specificity (32.5%–60.0%), whereas CTSF, MSLN, and MUC1 showed no diagnostic value (between-group $p > 0.2$). In contrast, sFRP4, FBLN1, and KLK6 demonstrated superior diagnostic performance (Figure 4B, Table 3). sFRP4 yielded an AUC of 0.743 (95% CI, 0.635–0.852), with a sensitivity of 86.8% and a specificity of 52.5% at a cutoff of 7.608 ng/mL. FBLN1 yielded an AUC of 0.727 (95% CI, 0.614–0.840), with a sensitivity of 84.2% and a specificity of 52.5% at a cutoff of 19.442 ng/mL. Notably, CSF KLK6 showed near-complete separation of the LCBM group from all control subgroups: 33 of the 38 LCBM values fell below all 40 control values (LCBM range 0.90–2.28 ng/mL vs. 2.07–2.56 ng/mL), yielding an AUC of 0.969 (95% CI, 0.935–1.000); at a cutoff of 2.061 ng/mL, KLK6 achieved a sensitivity of 86.8% and a specificity of 100%, the strongest single discriminator for LCBM diagnosis in this cohort (Supplementary Table 8). Because all control samples were recruited at one center, we repeated the comparison within that center; KLK6 retained high accuracy in the 7 Dalian patients (AUC 0.943; 1.664–2.241 vs 2.066–2.563 ng/mL; p < 0.001) as well as in the 31 patients recruited at Beijing (AUC 0.975), although absolute concentrations were higher in the Dalian patients (median 1.87 vs 1.47 ng/mL; p = 0.015), so that the discrimination was not confined to the cross-center comparison (Supplementary Table 6). Because CSF protein levels might be disproportionately influenced by lesions in direct contact with the CSF space, we performed a sensitivity analysis excluding the two patients with intraventricular metastases (Nos. 15 and 36; 5.3%). The discrimination of KLK6 was essentially unchanged (remaining 36 LCBM: AUC 0.967; range 0.898–2.278 ng/mL vs. 40 controls: 2.066–2.563 ng/mL; p < 0.001); the two excluded patients had KLK6 concentrations of 1.339 and 1.311 ng/mL, both below the control range, and the AUCs of sFRP4 (0.735) and FBLN1 (0.726) were likewise essentially unchanged, indicating that the discriminatory performance was not driven by CSF-contacting lesions.

Evaluation of Combined Diagnostic Models

To further enhance diagnostic accuracy, we constructed combined models using penalized binary logistic regression (model coefficients and bootstrap-corrected performance in Supplementary Table 9; Figure 4C, Table 4). All KLK6-containing combinations achieved near-perfect discrimination (apparent AUC 0.980–0.989), which was essentially unchanged after optimism correction by internal validation with bootstrapping (1,000 resamples; optimism-corrected AUC 0.977–0.986). The KLK6-free sFRP4 + FBLN1 combination showed an apparent AUC of 0.797 (95% CI, 0.697–0.897), with an optimism-corrected AUC of 0.791, outperforming either protein alone. Calibration analysis, however, revealed calibration slopes exceeding unity (2.5 for FBLN1 + KLK6; 2.6 for sFRP4 + FBLN1 + KLK6) with Brier scores of 0.059 and 0.049, respectively (Supplementary Figure 2), indicating that the ridge-penalized models yield conservative (under-confident) probabilities rather than well-calibrated ones, and that recalibration will be required in external cohorts. Given that the models were developed and evaluated within the same cohort, and that such near-perfect discrimination may not generalize to other populations, these findings should be regarded as preliminary, and independent external validation in a larger multicenter cohort is warranted.

CSF POSTN Predicts Poor Prognosis in LCBM

Bioinformatic Analysis of POSTN in Public Lung Cancer Datasets: Biological Context for a Prognostic Candidate

To provide biological context for the CSF findings, we interrogated public transcriptomic data from The Cancer Genome Atlas (TCGA) for the candidate biomarkers (Figure 5A). In unselected lung cancer cohorts, higher POSTN mRNA expression was associated with unfavorable overall survival (HR = 1.22, 95% CI 1.07–1.39; $p = 0.0023$), whereas the other candidates examined (KLK6, CTSF, and MSLN) showed weaker or non-significant associations. Because the candidates were ranked only according to the significance of their individual associations and no formal comparison of their discriminative ability was performed, these exploratory analyses do not establish POSTN as the strongest prognostic candidate among them. POSTN mRNA levels were higher in lung cancer tissues than in unpaired normal tissues ($p < 0.0001$; Figure 5B) and in paired adjacent normal samples ($p < 0.05$; Figure 5C), and Kaplan–Meier analysis of the TCGA cohort showed shorter survival among patients with high POSTN expression ($p < 0.05$; Figure 5D). These analyses were performed at the mRNA level in primary tumors from largely non-metastatic patients, and tumor mRNA abundance and CSF protein concentration are not necessarily correlated; they therefore provide supportive, rather than confirmatory, evidence for the CSF POSTN findings and should not be interpreted as independent validation of the prognostic value of CSF POSTN in LCBM.

Prognostic Validation of CSF POSTN in LCBM

We next evaluated the prognostic association of POSTN in the clinical LCBM cohort (n = 38, 32 deaths). Kaplan–Meier analysis stratified by CSF POSTN at the optimal cutoff (342.9 ng/mL, determined by maximally selected rank statistics; high, n = 19; low, n = 19) revealed that patients with high expression had significantly shorter overall survival than those with low expression (median OS, 19.0 vs. 51.0 months; log-rank $p < 0.001$, adjusted for cutoff selection; Cox HR = 6.13 for POSTN-high vs. POSTN-low, 95% CI 2.59–14.49, $p < 0.001$; Figure 5E). Because this cutoff was data-driven, POSTN was additionally analyzed as a continuous variable. In univariable Cox proportional hazards regression, each SD increase in log-transformed CSF POSTN was significantly associated with shorter overall survival (HR = 2.05, 95% CI 1.25–3.37, $p = 0.005$), indicating that the association does not depend on the cutoff; the dichotomized estimate is nonetheless likely to be optimistic, as the cutoff was selected in the same data. In a multivariable Cox model strictly limited to two prespecified covariates, higher CSF POSTN remained associated with worse overall survival (HR = 2.53 per SD, 95% CI 1.44–4.46, $p = 0.001$) after adjustment for age (HR = 1.74 per SD, 95% CI 1.10–2.77, $p = 0.019$) and targeted therapy (HR = 0.56 for yes vs. no, 95% CI 0.25–1.26, $p = 0.163$); a parallel model replacing targeted therapy with the presence of a driver gene alteration yielded consistent results (POSTN HR = 2.54 per SD, 95% CI 1.47–4.40, $p = 0.001$) (Supplementary Table 10). The estimate was unchanged when recruiting center was added to the model (per SD HR 2.71, 95% CI 1.56–4.72; $p < 0.001$); center itself was not associated with overall survival (HR 1.24, 95% CI 0.53–2.91; $p = 0.62$; likelihood-ratio test $p = 0.24$), and the association was reproduced within the 31 patients recruited at Beijing Chest Hospital (per SD HR 3.17, 95% CI 1.68–5.97; $p < 0.001$) (Supplementary Table 6). For comparison, CSF CEA dichotomized at its data-driven optimal cutoff (7.38 ng/mL; high, n = 23; low, n = 15) showed only a trend toward poorer prognosis that did not reach statistical significance (median OS, 31.0 vs. 61.0 months; nominal log-rank $p = 0.055$; $p = 0.34$ after adjustment for cutoff selection by permutation testing; Cox HR = 2.08 for high vs. low, 95% CI 0.96–4.52, $p = 0.064$; Figure 5F), and log-CEA was likewise not significant in continuous analysis (HR = 1.26 per SD, 95% CI 0.91–1.75, $p = 0.165$). We therefore formally compared the two markers instead of relying on the significance of each. Taken together, the discriminative ability of CSF POSTN was higher than that of CSF CEA in this cohort (ΔC-index 0.171, 95% CI 0.016–0.303), while the difference in the 36-month time-dependent AUC was not significant (ΔAUC 0.141, 95% CI −0.120–0.386); given the small sample, these comparisons are exploratory and should not be read as establishing superiority (Supplementary Tables 6 and 10). The findings should be interpreted as an association between CSF POSTN and overall survival rather than evidence of an independent prognostic factor, and both the continuous association and the dichotomization of POSTN require validation in an independent cohort.

Discussion

Lung cancer is among the most common malignancies worldwide, and brain metastasis remains a leading cause of death in these patients. Because cerebrospinal fluid (CSF) bathes the metastatic niche, it reflects the molecular characteristics of intracranial lesions more directly than peripheral blood, and it samples a compartment with a distinct immune landscape shaped by resident microglia, astrocytes and infiltrating immune cells[22]. Mass spectrometry-based proteomics allows sensitive profiling from minimal sample volumes and has been widely applied in lung cancer research [23][24] ; we therefore used CSF proteomics to identify candidate biomarkers of LCBM. This is a biomarker-discovery study: no immune-cell composition, T-cell function, macrophage polarization, PD-L1 expression or cytokine measurement was performed in our cohort, and the immunological framing below is drawn from published work and is hypothesis-generating rather than evidence generated here.

Four proteins were carried forward for biological discussion: FBLN1, KLK6, sFRP4 and POSTN; their proposed functions are derived from other tumor types and experimental systems, not from experiments reported here. FBLN1 is an extracellular matrix glycoprotein that regulates cell adhesion, vascular remodeling and tumor invasion[25][26][27][25] , and binds and regulates EGFR in lung cancer cells [28]. KLK6, a serine protease, is aberrantly expressed in several cancers, promotes growth, invasion and metastasis, and has been proposed as a diagnostic and prognostic biomarker [29] ; it has further been suggested to mediate crosstalk between cancer cells and macrophages [30]. sFRP4 modulates WNT signaling [31][32][33] , and aberrant WNT/β-catenin activation has been linked to immune exclusion and a “cold” tumor phenotype with impaired dendritic-cell recruitment and T-cell priming [34]. POSTN, secreted largely by cancer-associated fibroblasts, remodels the extracellular matrix, activates integrin–FAK/PI3K/AKT signaling and drives epithelial–mesenchymal transition [35][36] [37]; it has also been reported to skew macrophages towards an M2-like phenotype and to upregulate PD-L1[37] , and in lung cancer it contributes to EMT and apoptosis resistance [38] . Whether any of these mechanisms operates in LCBM was not examined here.

In the validation cohort, CSF sFRP4 was higher and FBLN1 and KLK6 were lower in patients with LCBM than in controls. These differences were consistent in direction across all five disease-control subgroups; after Holm–Bonferroni correction, however, only KLK6 remained significant against every subgroup, sFRP4 only against CNS lymphoma, and FBLN1 only against cerebral haemorrhage, which supports discrimination within a differential-diagnostic setting rather than specificity for brain metastasis. A combined sFRP4/FBLN1/KLK6 logistic model showed near-perfect discrimination after bootstrap internal validation (AUC 0.989; optimism-corrected 0.986), and sFRP4 + FBLN1 alone reached 0.791 after correction; both require independent external validation. Higher CSF POSTN was associated with shorter

overall survival (median 19.0 vs. 51.0 months; HR 6.13, 95% CI 2.59–14.49, p < 0.001); the association persisted when POSTN was modelled continuously (HR 2.05 per SD, 95% CI 1.25–3.37, p = 0.005) and after adjustment for age and targeted therapy (HR 2.53 per SD, 95% CI 1.44–4.46, p = 0.001), with a parallel model using driver-gene status giving consistent results (HR 2.54, 95% CI 1.47–4.40, p = 0.001). Because a significant association for one marker and a non-significant association for another does not itself establish a difference, discrimination was compared formally: the Harrell C-index was 0.749 for CSF POSTN and 0.577 for CSF CEA (difference 0.171, 95% CI 0.016–0.303), POSTN added prognostic information to a model containing CEA (likelihood-ratio p = 0.003) whereas CEA added none to POSTN (p = 0.160), but the difference in 36-month time-dependent AUC was not significant (0.776 vs. 0.635; difference 0.141, 95% CI −0.120 to 0.386) (Supplementary Table 10). These findings support further evaluation of CSF POSTN; they do not establish superiority over CEA.

The pattern of elevated sFRP4 with reduced FBLN1 and KLK6 is compatible with several interpretations. One is a shift towards WNT-driven immune exclusion and impaired matrix-mediated immune surveillance within the metastatic niche [39]; the same changes are equally compatible with non-immune explanations, including BBB disruption, stromal remodeling and systemic tumor burden, and distinguishing between them would require CSF protein measurement paired with direct immunological profiling [40]. A competing explanation requires particular attention. In 251 CSF samples across four brain-malignancy types, Schmid et al. showed that CSF proteome deregulation arises mainly from BBB disruption and is largely conserved across tumor entities [41]; KLK6 has likewise been described as a non-specific marker of neural injury and neuroinflammation, and all of our controls had active neurological disease [42]. Three observations argue against a purely barrier-derived signal. First, KLK6 concentrations were remarkably homogeneous across the five control subgroups (medians 2.21–2.35 ng/mL) and higher than in the LCBM group (median 1.43 ng/mL), with only 5 of 38 LCBM values overlapping the control range, whereas the subgroups with the most acute barrier breakdown (cerebral hemorrhage, encephalitis) were not the most extreme. Second, discrimination persisted after exclusion of the two patients with CSF-contacting intraventricular lesions (AUC 0.967). Third, the candidate-selection criteria explicitly favored changes reflecting tumor-specific biology over non-specific neural injury. A conclusive test would require controls without intracranial disease (see Limitations).

The absolute KLK6 concentrations measured here (0.9–2.6 ng/mL) are 10–100-fold lower than values reported with other assays (approximately 25.5 ng/mL in neurological controls and 220 ± 62 ng/mL in the normal controls of an Alzheimer cohort). Absolute concentrations are not directly comparable between ELISA kits, because antibody clones, calibrators and matrix handling differ; all values reported here fell within the calibration range of the kit used, but the

2.061 ng/mL cutoff is kit- and workflow-specific and must be re-established before it is transferred to other laboratories.

Our earlier studies implicated MSLN in LCBM using serum and tumor tissue [43] , and a serum and cell-line model based on CTSF and FBLN1 was associated with progression-free survival [44]. In the present CSF samples, however, neither MSLN nor CTSF differed between groups, whereas FBLN1 was significantly lower. Compartment-specific expression, the limited sample size and the selective permeability of the BBB, which restricts the entry of proteins and peripheral immune cells into the CNS [45], may all contribute to this discordance. These findings underscore the need for CSF-specific marker panels that account for the CNS-resident immune compartment rather than extrapolating from systemic biomarkers.

Several limitations qualify these findings. (i) No control group of patients with NSCLC without brain metastasis was included, because lumbar puncture is not clinically indicated in these patients and research-only sampling could not be approved by our ethics committee; the observed alterations therefore cannot be attributed specifically to brain metastasis rather than to lung cancer itself, advanced systemic malignancy or treatment exposure, and LCBM specificity is not established. (ii) No patient with leptomeningeal metastasis was included, so performance in, and discrimination from, leptomeningeal disease cannot be inferred. (iii) The diagnostic models were developed and internally validated in a single small cohort; independent external validation and recalibration of model probabilities are mandatory before clinical use. (iv) The prognostic analysis was performed in a small, clinically heterogeneous cohort (n = 38, 32 deaths) with adjustment limited to two prespecified covariates, and the dichotomization cutoff (342.9 ng/mL) was data-driven, with only 19 patients in each subgroup: the dichotomized HR of 6.13 is therefore likely to be optimistic and is reported with a wide confidence interval (2.59–14.49), although the log-rank p value was permutation-adjusted (p = 0.001) and the continuous association was robust. (v) The comparison between CSF POSTN and CSF CEA was inconsistent across metrics and does not support a claim of superiority. (vi) The TCGA analyses reflect POSTN mRNA in primary tumor tissue and survival in a largely non-metastatic population, and serve as biological context only. (vii) Survival was measured from the initial lung cancer diagnosis, whereas CSF was sampled at the brain-metastasis work-up; because only patients who survived long enough to undergo lumbar puncture could be enrolled, the cohort is subject to survivor enrichment and the medians reported here are not comparable with post-metastasis benchmarks. Such prolonged survival is nevertheless plausible given the enrichment for driver alterations (27/38, 71.1%; EGFR mutation 50.0%), for which median survival from first-line osimertinib approaches 38.6 months[46]. (viii) Pre-analytical variables may influence measured concentrations: handling was uniform (4 °C transport, centrifugation within 24 h, storage at −80 °C, single thaw, clarification before assay), but the collection-to-processing interval was not recorded, no blood-contamination index or dedicated CSF quality-control

marker was assessed, and samples were contributed by two centers in which center and case–control status were structurally related. The small case–control difference in POSTN was not reproduced within a single center (AUC 0.450, $p = 0.692$), so POSTN is reported as a prognostic rather than a diagnostic marker, whereas the survival association persisted after adjustment for center (HR 2.71 per SD, 95% CI 1.56–4.72). Age differed between groups ($p = 0.002$) and extracranial disease burden was not staged, so residual confounding cannot be excluded.

Larger, prospectively collected cohorts with center-balanced, age-matched controls and prospectively recorded pre-analytical variables are needed to validate these markers. The most informative next step would pair CSF protein measurement with direct immunological profiling — flow cytometry and single-cell RNA sequencing of CSF-infiltrating cells, together with paired tumor PD-L1 expression, T-cell infiltration and cytokine profiles — and would also allow CSF – serum correlations and blood-based alternatives to be explored. Integrating metastasis-specific markers with conventional lung cancer biomarkers and immune parameters may ultimately yield more practical diagnostic and prognostic models.

Conclusion

In conclusion, this study evaluated candidate biomarkers for the diagnosis and prognosis of LCBM by integrating CSF proteomics, ELISA validation, and bioinformatic analysis. First, KLK6, FBLN1, and sFRP4 were confirmed as significantly dysregulated CSF proteins: KLK6 discriminated LCBM from all disease-control subgroups after Holm–Bonferroni correction (AUC 0.969), and logistic models incorporating KLK6 maintained optimism-corrected AUCs of 0.977–0.986 after bootstrap internal validation, whereas the sFRP4 + FBLN1 combination achieved 0.791; given the limitations outlined above, these panels should be regarded as promising auxiliary tools for distinguishing LCBM from common neurological differential diagnoses rather than definitive diagnostic tests. Second, CSF POSTN showed exploratory prognostic value. Public TCGA transcriptomic data provided supportive biological context but, being mRNA-based and derived from largely non-metastatic primary tumors, do not validate the CSF findings. In our cohort, elevated CSF POSTN was associated with shorter overall survival both as a continuous variable (HR 2.05 per SD) and after adjustment for age and targeted therapy (HR 2.53 per SD), and in a formal head-to-head comparison POSTN showed higher discrimination than CEA (C-index 0.749 vs. 0.577), although the 36-month time-dependent AUC difference was not significant. Given the small prognostic cohort, the data-driven dichotomization, and the single-center design, POSTN should be viewed as an exploratory prognostic candidate whose advantage over CEA requires external confirmation rather than an established replacement. Overall, the KLK6/FBLN1/sFRP4 panel and CSF POSTN are candidate CSF biomarkers for the auxiliary diagnosis and prognostic evaluation of LCBM; these hypothesis-generating findings require independent external validation before clinical application.

Materials and Methods

Patient Selection and Cerebrospinal Fluid Collection

Discovery Cohort To identify biomarkers with high sensitivity and specificity for LCBM, we enrolled 56 subjects between August 2021 and August 2023 from the Department of Respiratory and Critical Care Medicine, Department of Thoracic Oncology and Department of Joint Surgery at The Second Hospital of Dalian Medical University, and from Beijing Chest Hospital, Capital Medical University. The discovery cohort comprised 28 patients with LCBM (23 from Beijing Chest Hospital, Capital Medical University and 5 from The Second Hospital of Dalian Medical University) and 28 non-tumor controls who underwent lumbar puncture for joint replacement surgery, all of whom were recruited at The Second Hospital of Dalian Medical University.

Validation Cohort Between August 2022 and August 2023, an additional 78 patients were recruited from the aforementioned departments, together with the Departments of Neurology, Neurosurgery and the Intensive Care Unit at The Second Hospital of Dalian Medical University, and from Beijing Chest Hospital, Capital Medical University. This cohort included 38 LCBM patients (31 from Beijing Chest Hospital, Capital Medical University and 7 from The Second Hospital of Dalian Medical University) and 40 neurological disease controls (11 primary intracranial tumors, 5 central nervous system lymphomas, 6 encephalitis, 12 cerebral hemorrhages and 6 epilepsy cases), all of whom were recruited at The Second Hospital of Dalian Medical University (Supplementary Tables 2 and 6).

Contribution of the two centers In total, 134 samples were analyzed, 80 contributed by The Second Hospital of Dalian Medical University and 54 by Beijing Chest Hospital, Capital Medical University (56 in the discovery cohort and 78 in the validation cohort), and none was excluded after collection. As a consequence of the recruitment structure of the two hospitals, all 68 control samples (28 in the discovery cohort and 40 in the validation cohort) were recruited at The Second Hospital of Dalian Medical University, whereas 54 of the 66 LCBM samples were recruited at Beijing Chest Hospital, Capital Medical University; the center of every patient is given in Supplementary Table 2 and the distribution is summarized in Supplementary Table 6. Both centers followed the same written standard operating procedure for collection, transport, centrifugation, aliquoting and storage, and all ELISA measurements were performed in a single laboratory on coded samples.

Inclusion and Exclusion Criteria Patients in the LCBM group had a histopathologically confirmed diagnosis of NSCLC with parenchymal brain metastasis demonstrated by contrast-enhanced MRI or CT. No patient had a clinical or radiological diagnosis of leptomeningeal metastasis, and no patient was enrolled on the basis of positive CSF cytology. Patients with any other systemic malignancy, severe hepatic or renal dysfunction, or uncontrolled systemic

infection were excluded, and all participants were ≥ 18 years old and provided written informed consent for lumbar puncture. Control patients had clinical indications for lumbar puncture or intracranial surgery, were ≥18 years old, and provided informed consent. CSF samples were collected during hospitalization approximately one month after the initial diagnosis of brain metastasis and before the initiation of any anti-tumor treatment for brain metastasis (chemotherapy, radiotherapy, targeted therapy or immunotherapy). For the non-tumor controls in the discovery cohort, lumbar puncture was not performed for research purposes: these patients were scheduled for elective joint arthroplasty under subarachnoid (spinal) anesthesia, for which a lumbar puncture is an integral part of the standard anesthetic procedure. A 2–3 mL aliquot of CSF was collected through the anesthesia needle at the time of this clinically indicated puncture, immediately before injection of the local anesthetic; no additional or research-only puncture was performed in any participant, and no procedure carried any risk beyond that of the clinically indicated anesthesia. This study was approved by the Ethics Committee of The Second Hospital of Dalian Medical University (Approval No. 227/2023), and written informed consent was obtained from all participants prior to sample collection.

CSF Collection and Processing CSF was collected by lumbar puncture under strict aseptic conditions. The first tube was discarded, the second was used for routine clinical tests, and the third was reserved for this study. Samples were sealed, transported and kept at 4 °C and, within 24 h of collection, were subjected to an initial centrifugation (5,000 × g for 10 min at 4 °C) to remove cells and debris. The supernatant was aliquoted in 0.5 mL volumes and stored at −80 °C until analysis. Immediately before analysis, each aliquot was thawed once and clarified by a second centrifugation (13,960 × g for 5 min at 4 °C); aliquots were not refrozen, so that all measurements were made on material that had undergone a single freeze–thaw cycle. Only clear, uniform CSF was accepted: samples showing red or yellow discoloration or turbidity were excluded at collection. CSF total protein, which is measured during routine clinical testing, was not used as a normalizer or as a quality-control metric because it varies widely between individuals and is itself influenced by the indication for lumbar puncture; concentrations are therefore reported as absolute values (ng/mL) obtained with the same calibrated ELISA kits, with two technical replicates averaged and samples randomized across plates.

Proteomic Analysis of CSF

Protein Extraction and Digestion Protein concentration was quantified for each sample. An aliquot containing 60 μg of protein was mixed with six volumes of denaturation buffer (6 M GdmCl, 50 mM HEPES, 40 mM CAA, 10 mM TCEP, pH 7.4). The mixture was vortexed and heated at 95°C for 5 min to reduce disulfide bonds and alkylate free thiols. Proteins were then transferred to 10 kDa ultrafiltration tubes and centrifuged at 13,960 × g at 4°C until dry. The filter was washed twice with 150 μL of 50 mM NH_4HCO_3 (pH 7.8). Trypsin (1/20 of the protein mass) was added in 200 μL of 50 mM NH_4HCO_3, and the mixture was incubated overnight at

37°C. Peptides were collected by centrifugation, and the filter was rinsed once with 200 μL of ultrapure water. The combined filtrates were lyophilized and stored at -20°C.

LC–MS/MS acquisition and quality control Peptides were reconstituted in 0.1% formic acid, and peptide concentrations were measured using a NanoDrop micro-spectrophotometer. Liquid chromatography–tandem mass spectrometry (LC–MS/MS) was performed on a Q Exactive H F mass spectrometer coupled to an Ultimate 3000 liquid chromatography system (Thermo Fisher Scientific). Peptides were separated on a homemade capillary column (35 cm × 50 μm inner diameter, 1.9 μm C18) at 55 °C over a 90-min gradient using mobile phase A (0.1% formic acid in water) and mobile phase B (0.1% formic acid in 80% acetonitrile). Each CSF sample was analyzed in technical duplicate, and the mean intensity of the two replicates was used for subsequent analysis. To minimize batch effects, all samples were injected in a randomized order with respect to group assignment.

Database search and protein identification Raw data files were searched against the UniProt human database (20,618 entries) using Spectronaut software in library-free directDIA mode. Peptide and protein identifications were both controlled at a false discovery rate (FDR) of 1%.

Quantitative data processing Quantitative data were preprocessed using a standard label-free proteomics workflow. Protein intensity values were log2-transformed to compress the dynamic range and to approximate a normal distribution, and the resulting intensity distributions of all samples were inspected to verify overall distribution trends and sample quality. Intensities were then normalized by median subtraction to reduce systematic variation between samples. Samples were assigned to the LCBM or control group and annotated accordingly. Proteins with fewer than 28 valid quantification values were regarded as insufficiently quantified and removed from further analysis. The remaining missing values were imputed by random sampling from a normal distribution (width = 0.3 SD, downshift = 1.8 SD) to simulate signals of low-abundance proteins.

Statistical analysis Differential protein abundance between the LCBM and control groups was assessed using a two-sample Student's t-test, and the resulting p values were adjusted for multiple testing using the permutation-based FDR approach. For baseline characteristics, continuous variables are presented as mean ± standard deviation and were compared using Student's t-test, whereas categorical variables are presented as n (%) and were compared using Pearson's chi-square test. Statistical analyses were performed using Perseus[47] and GraphPad Prism software. $p < 0.05$ was considered statistically significant; exact p values are reported in the tables, and thresholds such as $p < 0.05$ are used only where individual values are not tabulated (for example, for the 1,674 proteins of the discovery proteomic screen).

Enzyme-Linked Immunosorbent Assay (ELISA) Commercial pre-coated sandwich ELISA kits were used (Jianglai Biological, Shanghai, China; the CTSF kit was from Omnimabs, Alhambra, CA, USA), and all assays were performed strictly according to the manufacturers'

instructions. Standards and samples (5 μL per well, each in duplicate) were added to the antibody pre-coated wells, followed by the enzyme-conjugated detection reagent, and plates were incubated at 37 °C. After washing, chromogenic substrate was added, the reaction was stopped with the provided stop solution, and absorbance was measured at 450 nm within 15 min on a microplate reader (Rayto RT-6100). Concentrations were interpolated from each plate's standard curve, and all reported concentrations fell within the calibration range of the corresponding kit (Supplementary Table 8). The linear range, limit of detection, sample dilution factor, and intra- and inter-assay coefficients of variation of each kit were as specified in the manufacturers' instructions.

Clinical Statistical Analysis

Cohort Analysis Statistical analyses were performed using R software. All diagnostic groups consisted of independent subjects, and no paired analyses were performed. Normally distributed continuous variables are presented as mean ± standard deviation (SD) and were compared using independent samples t-tests (two groups) or one-way ANOVA (multiple groups). Non-normally distributed continuous variables are presented as median (interquartile range, IQR) or mean ± SD where appropriate, and group differences across the LCBM group and multiple control subgroups were assessed by one-way ANOVA or the Kruskal–Wallis H test, as applicable. For prespecified post-hoc comparisons of the LCBM group with each control subgroup, two-sided pairwise tests for independent samples were used — Dunnett's test following ANOVA, or Mann–Whitney U tests with Holm–Bonferroni step-down adjustment following the Kruskal–Wallis test — with the adjusted p values reported throughout. Categorical variables are presented as frequencies and percentages and were compared using Pearson's chi-square test. Recruiting center was structurally related to case–control status in this dataset, because all control samples were contributed by one of the two centers; center could therefore not be entered as a covariate in the case–control comparisons. The influence of center was instead examined directly: CSF POSTN was compared between LCBM and control samples within the single center that contributed both (7 LCBM vs 40 controls), and between LCBM patients from the two centers, using Mann–Whitney U tests with permutation-based p values (20,000 permutations) because of the small subgroup sizes. For the prognostic analysis, center was additionally entered as a covariate in the multivariable Cox models, its independent contribution was assessed by the likelihood-ratio test, and the analyses were repeated within the larger single-center subset. All center-stratified analyses are reported in Supplementary Table 6. Graphs, including bar charts, scatter plots, and ROC curves, were generated using GraphPad Prism.

Diagnostic Performance The diagnostic component of this study is reported in accordance with STARD 2015, and the multivariable diagnostic models are reported following the TRIPOD recommendations. Diagnostic efficacy was evaluated using ROC curve analysis. For individual

biomarkers, cutoff values were determined by maximizing the Youden index, with the corresponding sensitivity and specificity reported. For combined diagnostic models, binary logistic regression was used to fit multivariable diagnostic equations, and ROC analysis was subsequently performed on the predicted probabilities to assess diagnostic performance. To guard against overfitting and to obtain finite and stable coefficient estimates in this moderate-sized cohort, penalized (ridge) logistic regression was applied; model coefficients are reported in Supplementary Table 9. No sample-sizecalculation was performed for the diagnostic models; the cohort size was determined by the number of eligible patients recruited during the study period. No data were missing for any of the analytes included in the models, no imputation was required, and ELISA measurements were performed on coded samples without knowledge of the clinical group assignment. The reference standard for LCBM was the composite clinical diagnosis (histologically confirmed NSCLC with parenchymal brain metastasis on contrast-enhanced neuroimaging). The models were developed and evaluated in the same cohort without external validation, corresponding to TRIPOD type 2a; their performance should be considered preliminary pending independent external validation. The optimism of apparent model performance was quantified and corrected through internal validation with bootstrapping (1,000 resamples with replacement), and optimism-corrected AUCs with 95% confidence intervals were reported. Model calibration was assessed using calibration plots, the calibration slope and intercept, and the Brier score.

Survival Analysis Overall survival (OS) was defined as the interval from the date of the initial diagnosis of lung cancer to death from any cause or the date of the last follow-up; the data cut-off was June 2026. Kaplan–Meier survival analysis was conducted to evaluate the prognostic value of CSF POSTN and CSF CEA in the 38 LCBM patients with available survival data. The optimal cutoff values for CSF POSTN and CSF CEA were each determined using the surv_cutpoint function from the R package survminer (v0.4.9): all possible cutoffs were evaluated, and the optimal value was selected as the one maximizing the log-rank test statistic when comparing overall survival between the high- and low-expression groups, with a minimum proportion of 20% required for each group to ensure balanced group sizes (POSTN, 342.9 ng/mL; CEA, 7.38 ng/mL); the robustness of each optimal cutoff was verified using maximally selected rank statistics (maxstat package). Because this cutoff selection is data-driven and may introduce optimism bias, CSF POSTN was additionally analyzed as a continuous variable (log-transformed) in univariable Cox proportional hazards regression, with hazard ratios (HRs) expressed per SD increase. A multivariable Cox model, strictly limited to two prespecified covariates to preserve statistical stability given the sample size (n = 38, 32 events)—age and the administration of targeted therapy—was fitted to assess the association after adjustment for major clinical prognostic factors; a parallel model replaced targeted therapy with the presence of a driver gene alteration (EGFR mutation, ALK fusion, KRAS mutation, or RET rearrangement). Cox regressions were fitted with Breslow handling of tied event times,

and results are reported as HRs with 95% confidence intervals (Supplementary Table 10). All prognostic analyses are exploratory, and any dichotomization of POSTN requires validation in an independent cohort.

Materials and Reagents

The following reagents were utilized in this study. Saline (0.9% NaCl) was purchased from Shijiazhuang No. 4 Pharmaceutical Co., Ltd. (Shijiazhuang, China). PBS solution (0.01 M, pH 7.4) was obtained from Wuhan Pricella Biotechnology Co., Ltd. (Wuhan, China). Ammonium bicarbonate (NH4HCO3), Guanidine hydrochloride (6 M GdmCl), 4-(2-Hydroxyethyl) piperazine-1-ethanesulfonic acid (50 mM HEPES), Tris(2-carboxyethyl) phosphine (10 mM TCEP), 2-Chloroacetamide (CAA), Formic acid (FA, 98%), and Trypsin (bovine, TPCK-treated) were acquired from Sigma-Aldrich (St. Louis, MO, USA). Acetonitrile (ACN, HPLC grade) was supplied by Merck (Darmstadt, Germany). Deionized water was generated using a Milli-Q system (Millipore, Bedford, MA, USA). The Human Cathepsin F (CTSF) ELISA Kit was purchased from Omnimabs (Alhambra, CA, USA). ELISA kits for Human Mucin 1 (MUC1), Mesothelin (MSLN), Periostin (POSTN/OSF-2), Neutrophil Gelatinase-Associated Lipocalin (LCN2), Activated Leukocyte Cell Adhesion Molecule (ALCAM), Secreted Frizzled-Related Protein 4 (sFRP4), Fibulin-1 (FBLN1), and Kallikrein 6 (KLK6) were obtained from Jianglai Biological (Shanghai, China).

Acknowledgements

We thank all patients who participated in this study and their families. We also thank the staff of the Department of Respiratory and Critical Care Medicine, Department of Thoracic Oncology and Department of Joint Surgery at The Second Hospital of Dalian Medical University, and of Beijing Chest Hospital, Capital Medical University, for their assistance with patient recruitment and sample collection.

Authors' contributions

QW conceived and supervised the study and was responsible for the final interpretation of the results. YJ performed the sample collection and sample preparation and drafted the manuscript. YX performed the protein enrichment and database analyses and the survival analyses. WL critically revised and edited the manuscript. SW was responsible for sample collection and coordination at the Beijing Chest Hospital. XY supervised the study, finalized the manuscript, and improved its readability. MLY supervised the mass spectrometric analysis and verified the proteomic data. All authors read and approved the final manuscript.

Funding

This work was supported by the National Natural Science Foundation of China (Grant Nos. 82473056, 82027805 and 82303411), the Liaoning Clinical Medical Research Center Construction Program, the Dalian Respiratory Tract Protection Engineering Research Center, and the Capital's Funds for Health Improvement and Research (2024-4-2164). The funders had no role in study design, data collection and analysis, decision to publish, or preparation of the manuscript.

Competing interests

The authors declare that they have no competing interests.

Data Availability Statement

All data generated or analyzed during this study are included in this published article and its supplementary information files. The datasets generated during this study are fully available within the article and supplementary materials (Supplementary Tables).

Ethics approval and consent to participate

This study was approved by the Ethics Committee of The Second Hospital of Dalian Medical University (Approval No. 227/2023) and was conducted in accordance with the Declaration of Helsinki. Written informed consent for lumbar puncture and for the use of the cerebrospinal fluid samples in this study was obtained from all participants.

Consent for publication

Not applicable.

References

[1] Thai AA, Solomon BJ, Sequist LV, Gainor JF, Heist RS. Lung cancer. Lancet. 2021;398(10299):535-554. doi:10.1016/S0140-6736(21)00312-3

[2] Li S, Wang A, Wu Y, et al. Targeted therapy for non-small-cell lung cancer: New insights into regulated cell death combined with immunotherapy. Immunol Rev. 2024; 321: 300-334. doi:10.1111/imr.13274

[3] Siegel RL, Miller KD, Fuchs HE, Jemal A. Cancer Statistics, 2021. CA Cancer J Clin. 2021;71(1):7-33. doi:10.3322/caac.21654

[4] Ulahannan D, Khalifa J, Faivre-Finn C, Lee SM. Emerging treatment paradigms for brain metastasis in non-small-cell lung cancer: an overview of the current landscape and challenges ahead. Ann Oncol. 2017;28(12):2923-2931. doi:10.1093/annonc/mdx481

[5] Wu D, Deng S, Li L, et al. TGF-β1-mediated exosomal lnc-MMP2-2 increases blood-brain barrier permeability via the miRNA-1207-5p/EPB41L5 axis to promote non-small cell lung cancer brain metastasis. Cell Death Dis. 2021;12(8):721. Published 2021 Jul 20. doi:10.1038/s41419-021-04004-z

[6] Howlader N, Forjaz G, Mooradian MJ, et al. The Effect of Advances in Lung-Cancer Treatment on Population Mortality. N Engl J Med. 2020;383(7):640-649. doi:10.1056/NEJMoa1916623

[7] Vinicius Ernani et al. Management of Brain Metastases in Non–Small-Cell Lung Cancer. JOP 15, 563-570(2019). DOI:10.1200/JOP.19.00357

[8] Wolpert F, Lareida A, Terziev R, et al. Risk factors for the development of epilepsy in patients with brain metastases. Neuro Oncol. 2020;22(5):718-728. doi:10.1093/neuonc/noz172

[9] Le Rhun E, Guckenberger M, Smits M, et al. EANO-ESMO Clinical Practice Guidelines for diagnosis, treatment and follow-up of patients with brain metastasis from solid tumors. Ann Oncol. 2021;32(11):1332-1347. doi:10.1016/j.annonc.2021.07.016

[10] Alix-Panabières C, Pantel K. Liquid Biopsy: From Discovery to Clinical Application. Cancer Discov. 2021;11(4):858-873. doi:10.1158/2159-8290.CD-20-1311

[11] Bertero L, Siravegna G, Rudà R, Soffietti R, Bardelli A, Cassoni P. Review: Peering through a

keyhole: liquid biopsy in primary and metastatic central nervous system tumors. Neuropathol Appl Neurobiol. 2019;45(7):655-670. doi:10.1111/nan.12553

[12] Naidoo J, Schreck KC, Fu W, et al. Pembrolizumab for patients with leptomeningeal metastasis from solid tumors: efficacy, safety, and cerebrospinal fluid biomarkers. Journal for Immunotherapy of Cancer. 2021 Aug;9(8):e002473. DOI: 10.1136/jitc-2021-002473. PMID: 34380662; PMCID: PMC8359453.

[13] Mattox AK, Yan H, Bettegowda C. The potential of cerebrospinal fluid-based liquid biopsy approaches in CNS tumors. Neuro Oncol. 2019;21(12):1509-1518. doi:10.1093/neuonc/noz156

[14] Masmoudi D, Alix-Panabières C, Eslami-S Z. Integrating immunopeptidomics with liquid biopsy for precision oncology. Mol Aspects Med. 2026;110:101478. doi:10.1016/j.mam.2026.101478

[15] Du, X., Li, E., Wang, Q. et al. A Bird's Eye View of Quantitative Proteome of Tumor Tissues from Lung Cancer Patients by a High Precision Mass Spectrometry Method. Chem. Res. Chin. Univ. 40, 136–144 (2024). https://doi.org/10.1007/s40242-024-3246-y

[16] Schmid D, Warnken U, Latzer P, et al. Diagnostic biomarkers from proteomic characterization of cerebrospinal fluid in patients with brain malignancies. J Neurochem. 2021; 158: 522–538. https://doi.org/10.1111/jnc.15350

[17] De Mattos-Arruda, L., Mayor, R., Ng, C. et al. Cerebrospinal fluid-derived circulating tumor DNA better represents the genomic alterations of brain tumors than plasma. Nat Commun 6, 8839 (2015). https://doi.org/10.1038/ncomms983

[18] Wei S, Liu W, Xu M, et al. Cathepsin F and Fibulin-1 as novel diagnostic biomarkers for brain metastasis of non-small cell lung cancer. Br J Cancer. 2022;126(12):1795-1805. doi:10.1038/s41416-022-01744-3

[19] Fu M, Zhao J, Zhang L, et al. Overcoming tyrosine kinase inhibitor resistance in lung cancer brain metastasis with CTLA4 blockade. Cancer Cell. 2024;42(11):1882-1897.e7. doi:10.1016/j.ccell.2024.09.012

[20] Yang JJ, Wen W, Zahed H, et al. Lung Cancer Risk Prediction Models for Asian Ever-Smokers. J Thorac Oncol. 2024;19(3):451-464. doi:10.1016/j.jtho.2023.11.002

[21] Rami-Porta R, Nishimura KK, Giroux DJ, et al. The International Association for the Study of Lung Cancer Lung Cancer Staging Project: proposals for revision of the TNM stage groups in the forthcoming (ninth) edition of the TNM classification for lung cancer. J Thorac Oncol. 2024;19(7):1007-1027. doi:10.1016/j.jtho.2024.02.011

[22] Liu Y, Yang F, Jin Y, et al. Dual immunometabolic regulation and therapeutic targeting of TAMs, microglia and astrocytes in brain metastasis of non-small cell lung cancer. Biochim Biophys Acta Rev Cancer. 2026;1881(4):189601. doi:10.1016/j.bbcan.2026.189601

[23] Lee GK, Lee HS, Park YS, et al. Lipid MALDI profile classifies non-small cell lung cancers according to the histologic type. Lung Cancer. 2012;76(2):197-203. doi:10.1016/j.lungcan.2011.10.016

[24] Jianyong Z, Yanruo H, Xiaoju T, et al. Roles of Lipid Profiles in Human Non-Small Cell Lung

Cancer. Technol Cancer Res Treat. 2021;20:153. doi:10.1177/15330338211041472

[25] Gong J, Jie Y, Xiao C, et al. Increased Expression of Fibulin-1 Is Associated With Hepatocellular Carcinoma Progression by Regulating the Notch Signaling Pathway. Front Cell Dev Biol. 2020;8:478. Published 2020 Jun 16. doi:10.3389/fcell.2020.00478

[26] Williams SA, Schwarzbauer JE. A shared mechanism of adhesion modulation for tenascin-C and fibulin-1. Mol Biol Cell. 2009;20(4):1141-1149. doi:10.1091/mbc.e08-06-0621

[27] Xu Z, Chen H, Liu D, et al. Fibulin-1 is downregulated through promoter hypermethylation in colorectal cancer: a CONSORT study. Medicine (Baltimore). 2015;94(13):e663. doi:10.1097/MD.0000000000000663

[28] Harikrishnan K, Joshi O, Madangirikar S and Balasubramanian N (2020) Cell Derived Matrix Fibulin-1 Associates With Epidermal Growth Factor Receptor to Inhibit Its Activation, Localization and Function in Lung Cancer Calu-1 Cells. Front. Cell Dev. Biol. 8:522. doi: 10.3389/fcell.2020.00522

[29] Martial S. Involvement of ion channels and transporters in carcinoma angiogenesis and metastasis. Am J Physiol Cell Physiol. 2016;310(9):C710-C727. doi:10.1152/ajpcell.00218.2015

[30] Hwang YS, Cho HJ, Park ES, et al. KLK6/PAR1 axis promotes tumor growth and metastasis by regulating cross-talk between tumor cells and macrophages. Cells. 2022;11(24):4101. doi:10.3390/cells11244101

[31] Pawar NM, Rao P. Secreted frizzled related protein 4 (sFRP4) update: a brief review. Cell Signal. 2018;45:63-70. doi:10.1016/j.cellsig.2018.01.019

[32] Deshmukh A, Arfuso F, Newsholme P, et al. Epigenetic demethylation of sFRPs, with emphasis on sFRP4 activation, leading to Wnt signalling suppression and histone modifications in breast, prostate, and ovary cancer stem cells. Int J Biochem Cell Biol. 2019;109:23-32. doi:10.1016/j.biocel.2019.01.016

[33] Natarajan A, Bandla SS, Damodaran M, et al. Study on the SFRP4 gene polymorphism and expression in prostate cancer. J Genet. 2020;99(1). doi:10.1007/s12041-020-01247-1

[34] Haseeb M, Pirzada RH, Ain QU, et al. Wnt signaling in the regulation of immune cell and cancer therapeutics. Cells. 2019;8(11):1380. doi:10.3390/cells8111380

[35] Liu X, Yao Q, Wang Z, et al. POSTN+ CAFs facilitate gastric cancer peritoneal metastasis by promoting ICAM-1-dependent tumor cell adhesion and CD8+ T-cell exhaustion. Front Immunol. 2026;17:1796080. Published 2026 Jun 10. doi:10.3389/fimmu.2026.1796080

[36] Tashireva LA, Grigoryeva ES, Patskan IA, Kalinchuk AY, Zelchan RV. Spatial Analysis of FAP Gene Expression in Breast Cancer. Curr Cancer Drug Targets. Published online June 19, 2026. doi:10.2174/0115680096433584260407101537

[37] Zhou Y, Yu JH, Sui QQ, et al. POSTN+ cancer-associated fibroblasts forming fortress-like barrier to mediate immunotherapy resistance in colorectal cancer. Cancer Lett. Published online June 17, 2026. doi:10.1016/j.canlet.2026.218683

[38] Sun D, Chen X, Lu J, et al. The impact of POSTN on tumor cell behavior and the tumor

microenvironment in lung adenocarcinoma. Int Immunopharmacol. 2025;145:113713. doi:10.1016/j.intimp.2024.113713

[39] [39] Spranger S, Bao R, Gajewski TF. Melanoma-intrinsic β-catenin signalling prevents anti-tumor immunity. Nature. 2015;523(7559):231-235. doi:10.1038/nature14404

[40] [40] Ampie L, McGavern DB. Immunological defense of CNS barriers against infections. Immunity. 2022;55(5):781-799. doi:10.1016/j.immuni.2022.04.012

[41] [41] Schmid D, Warnken U, Latzer P, et al. Diagnostic biomarkers from proteomic characterization of cerebrospinal fluid in patients with brain malignancies. J Neurochem. 2021; 158: 522–538. https://doi.org/10.1111/jnc.15350

[42] [42] Mella C, et al. Involvement of kallikrein-related peptidases in nervous system disorders. Front Cell Neurosci. 2020;14:166. doi:10.3389/fncel.2020.00166

[43] Xia S, Duan W, Xu M, et al. Mesothelin promotes brain metastasis of non-small cell lung cancer by activating MET. J Exp Clin Cancer Res. 2024;43(1):103. doi:10.1186/s13046-024-03015-w

[44] Jiang Q, Yu W, Ma J, et al. Robust differentiation of NK cells from MSLN.CAR-IL-15-engineered human iPSCs with enhanced antitumor efficacy against solid tumors. Sci Adv. 2025;11(18):eadt9932. doi:10.1126/sciadv.adt9932

[45] Ampie L, McGavern DB. Immunological defense of CNS barriers against infections. Immunity. 2022;55(5):781-799. doi:10.1016/j.immuni.2022.04.012

[46] Ramalingam SS, Vansteenkiste J, Planchard D, Cho BC, Gray JE, Ohe Y, et al. Overall Survival with Osimertinib in Untreated, EGFR-Mutated Advanced NSCLC. N Engl J Med. 2020;382(1):41-50. doi: 10.1056/NEJMoa1913662

[47] Tyanova S, Temu T, Sinitcyn P, et al. The Perseus computational platform for comprehensive analysis of (prote)omics data. Nat Methods. 2016;13(9):731-740. doi:10.1038/nmeth.3901

Table 1. Baseline demographic and clinical characteristics of the discovery cohort (A) and validation (B) cohorts.

A. Discovery cohort (LCBM group vs. control group)

Characteristics		LCBM Group	Control Group	Pearson Chi-Square	Variance	*P* value
Sample		28	28		-	
Age	Mean	58.89	65.64	-	0.51	0.002
	Standard Deviation	7.305	8.010			
	Shapiro-Wilk test	0.458	0.625		-	
Gender	Male	12 (42.9%)	9 (32.1%)	0.686	-	0.408
	Female	16 (57.1%)	19(67.9%)			

Continuous variables are presented as mean ± standard deviation. Normality was assessed by the Shapiro–Wilk test. Age was compared between groups using Student's t-test for independent samples (Levene's test for equality of variances, $p = 0.51$), and categorical variables (sex) were compared using Pearson's chi-square test. $p < 0.05$ was considered statistically significant.
LCBM Group: Patients with brain metastases from non-small cell lung cancer.

B. Validation cohort.

Characteristics		LCBM Group (n = 38)	Control Group (n = 40)					Statistics	*P* value
			Primary intracranial tumor (n = 11)	Lymphoma (n = 5)	Encephalitis (n = 6)	Intracerebral hemorrhage (n = 12)	Epilepsy (n = 6)		
Age	Mean	61.921	55.000	52.600	53.167	60.750	50.500	*F*=1.473	0.209
	SD	8.747	13.689	20.513	20.164	13.778	23.923		
	95%CI	59.046-64.796	45.803-64.197	27.123-78.071	32.006-74.327	51.996-69.504	25.395-75.605		
Gender	Male	19（50.0%）	6（54.5%）	3 (60.0%)	3（50.0%）	10 (83.3%)	4 (66.7%)	χ^2=4.553	0.473
	Female	19（50.0%）	5（45.5%）	2 (40.0%)	3（50.0%）	2 (16.7%)	2 (33.3%)		

Data are presented as mean ± SD for continuous variables and n (%) for categorical variables. Differences in age across groups were analyzed using one-way ANOVA, while gender distribution was compared using the Chi-square test. p value < 0.05 was considered statistically significant.

Abbreviations: LCBM, Patients with brain metastases from non-small cell lung cancer; SD, standard deviation; ANOVA, analysis of variance.

Table 2. CSF concentrations of target proteins in the LCBM group and control groups of the validation cohort.

A. LCBM group versus all controls

Protein Name		LCBM Group (ng/mL)	Control Group (ng/mL)	*p* value
CTSF	Mean	300.397	302.629	0.798
	95% CI	288.826~311.968	289.530~315.728	
MSLN	Mean	4.0856	3.515	0.242
	95% CI	3.417~4.754	2.804~4.227	
MUC1	Mean	12.308	12.431	0.960
	95% CI	9.947~14.670	8.204~16.657	
POSTN	Mean	343.122	311.712	0.045
	95% CI	328.702~357.542	284.531~338.892	
ALCAM	Mean	40.134	29.832	<0.001
	95% CI	36.953~43.316	25.036~34.628	
LCN2	Mean	58.695	46.289	0.001
	95% CI	54.799~62.591	40.156~52.422	
sFRP4	Mean	10.437	7.786	<0.001
	95% CI	9.264~11.610	6.850~8.722	
FBLN1	Mean	12.134	29.541	0.005
	95% CI	8.692~15.577	18.071~41.010	
KLK6	Mean	1.608	2.300	<0.0001
	95% CI	1.487~1.730	2.258~2.342	

Data are presented as mean concentration (ng/mL) with 95% confidence intervals (95% CI). Statistical significance was determined by comparing the two groups, with p values < 0.05 considered statistically significant. Bolded proteins indicate those with significant differential expression.

LCBM: Lung Cancer Brain Metastasis; CTSF: Cathepsin F; MSLN: Mesothelin; MUC1: Mucin 1; POSTN: Periostin; ALCAM: Activated Leukocyte Cell Adhesion Molecule; LCN2: Lipocalin-2; sFRP4: Secreted Frizzled Related Protein 4; FBLN1: Fibulin-1; KLK6: Kallikrein Related Peptidase 6.

B. Concentrations of sFRP4, FBLN1, and KLK6 in the LCBM group and the five control subgroups

Group	n	sFRP4		FBLN1		KLK6	
		Mean	SD	Mean	SD	Mean	SD
LCBM	38	10.437	3.569	12.134	10.473	1.608	0.369
Primary intracranial tumor	11	7.662	2.037	18.028	15.877	2.331	0.146
CNS lymphoma	5	5.986	1.564	83.559	78.426	2.313	0.154
Encephalitis	6	9.910	4.799	22.709	12.790	2.221	0.049
Cerebral hemorrhage	12	7.906	2.825	28.038	19.739	2.291	0.156
Epilepsy	6	7.153	2.600	15.468	8.807	2.329	0.057
Overall ANOVA, *F (5, 72)*		**3.470**		**9.207**		**23.919**	
***p* value**		**0.007**		**< 0.001**		**< 0.001**	

Data are presented as mean (95% CI) in panel A and mean ± SD in panel B; concentrations are given in ng/mL. In panel A, bolded proteins indicate significant differential expression. In panel B, differences among the six diagnostic groups were assessed by one-way ANOVA (F statistic with degrees of freedom in parentheses). Prespecified post-hoc comparisons of the LCBM group with each control subgroup were performed using two-sided Mann–Whitney U tests for independent samples, and p values were adjusted for multiple comparisons across the five subgroup contrasts using the Holm–Bonferroni step-down procedure; the adjusted p values are given in Supplementary Table 7, and $p < 0.05$ was considered statistically significant. No paired tests were used, as all groups consisted of independent subjects. The five control subgroups together constituted the combined disease-control group ($n = 40$) used for the ROC analyses presented in Tables 3 and 4. Notably, 33 of the 38 LCBM values of KLK6 were lower than every control value, and KLK6 was significantly lower in the LCBM group than in every control subgroup (all Holm-adjusted $p < 0.001$; Supplementary Table 7). The encephalitis subgroup showed an exceptionally narrow KLK6 distribution (SD = 0.049 ng/mL, CV = 2.2 %); the six raw values (2.154–2.290 ng/mL; median 2.208 ng/mL, IQR 2.198–2.251) were re-verified against the primary plate data, and the tight distribution was confirmed.

Table 3. ROC curve analysis of the diagnostic performance of candidate biomarkers for LCBM.

Protein Name	Direction in LCBM	AUC (95%CI)	*p* value	Optimal Cutoff	Youden Index	Sensitivity (%)	Specificity (%)
POSTN	↑	0.572 0.443-0.701	0.276	293.158	0.272	94.7	32.5
ALCAM	↑	0.735 0.619-0.851	<0.001	30.702	0.495	89.5	60.0
LCN2	↑	0.679 0.560-0.797	0.007	42.924	0.347	94.7	40.0
sFRP4	↑	0.743 0.635-0.852	<0.001	7.608	0.393	86.8	52.5
FBLN1	↓	0.727 0.614-0.840	<0.001	19.442	0.367	84.2	52.5
KLK6	↓	0.969 0.935-1.000	<0.001	2.061	0.868	86.8	100.0

AUC, area under the ROC curve; CI, confidence interval. Cutoff values were determined by maximizing the Youden index (sensitivity + specificity − 1). "Direction in LCBM" indicates whether the protein was upregulated (↑) or downregulated (↓) in the LCBM group relative to the non-LCBM controls; for downregulated proteins, sensitivity was defined as the proportion of LCBM patients with concentrations below the cutoff, and specificity as the proportion of controls above the cutoff. p values refer to the test of AUC = 0.5. The 95% CIs for sFRP4, FBLN1, and KLK6 were obtained by the DeLong method. CSF KLK6 showed near-complete separation of the LCBM group from the non-LCBM controls (33 of 38 LCBM values below all 40 control values; 47 discordant pairs among 1,520 case–control comparisons). POSTN, ALCAM, and LCN2 were measured in the same assay batch; their estimates are shown for comparison. $p < 0.05$ was considered statistically significant.

Table 4. Diagnostic performance of the combined biomarker models for LCBM.

Combined Model	Apparent AUC (95%CI)	Optimism-corrected AUC[1]	*p* value	Cutoff (probability)[2]	Youden Index	Sensitivity (%)	Specificity (%)
sFRP4+FBLN1+KLK6	0.989 0.976-1.000	0.986	<0.001	0.440	0.896	92.1	97.5
FBLN1+KLK6	0.984 0.958-1.000	0.982	<0.001	0.302	0.924	97.4	95.0
sFRP4+KLK6	0.980 0.955-1.000	0.977	<0.001	0.394	0.896	92.1	97.5
sFRP4+FBLN1	0.797 0.697-0.897	0.791	<0.001	0.536	0.511	71.1	80.0

Combined models were constructed by penalized (ridge) binary logistic regression using the CSF concentrations of the indicated proteins as covariates; ROC analysis was performed on the model-predicted probabilities. Model coefficients are provided in Supplementary Table 9. Cutoff values represent probability thresholds maximizing the Youden index. [1]Optimism-corrected AUCs were obtained by internal validation with bootstrapping (1,000 resamples with replacement); the apparent AUC minus the mean optimism yields the corrected estimate. For models containing KLK6, apparent AUCs ranged from 0.980 to 0.989 and optimism-corrected AUCs from 0.977 to 0.986. The calibration of these models is presented in Supplementary Figure 2; calibration slopes exceeding unity reflect the shrinkage of the ridge-penalized coefficients, i.e., conservative (under-confident) predicted probabilities. As the models were developed and evaluated within the same cohort, their performance should be considered preliminary pending independent external validation. p values refer to the test of AUC = 0.5. $p < 0.05$ was considered statistically significant.

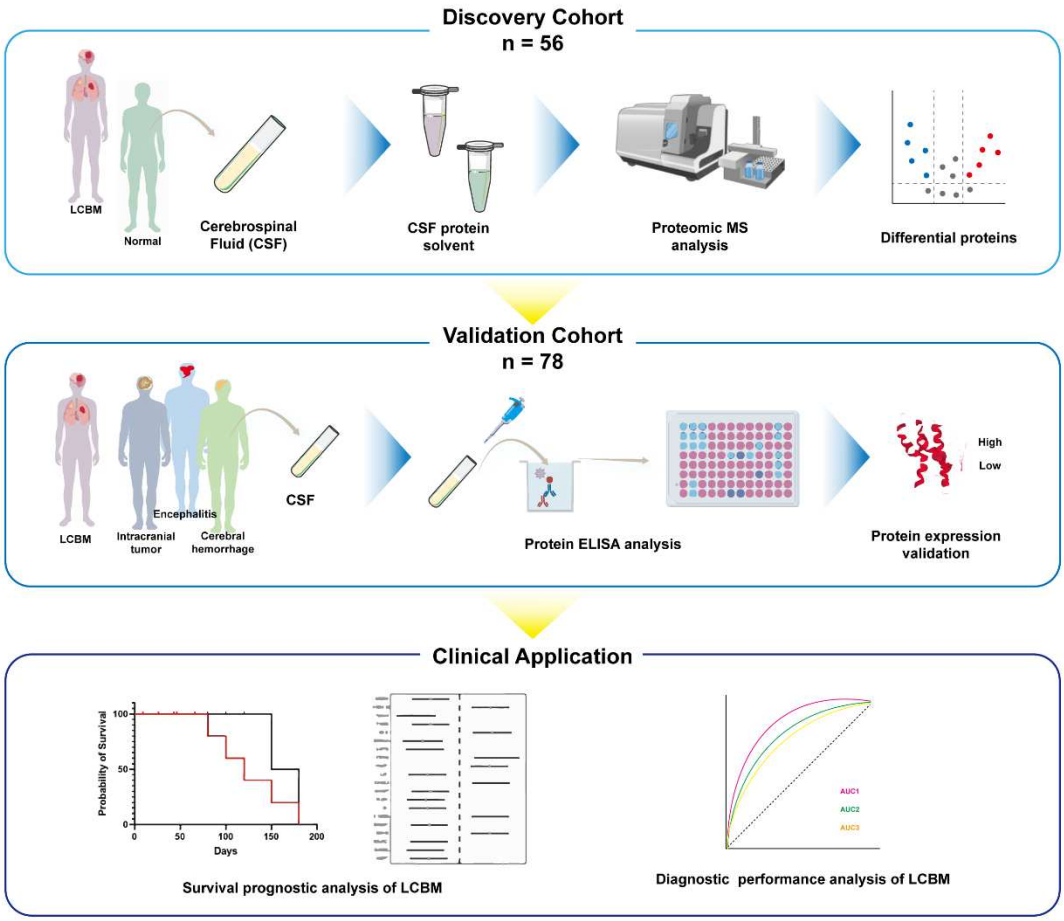


Figure 1. Schematic overview of the study design and workflow.

The study was conducted in three phases: discovery, analytical validation, and prognostic evaluation. In the Discovery Cohort (n = 56), CSF samples were collected from patients with LCBM and non-tumor controls undergoing spinal anesthesia for joint arthroplasty. Proteomic mass spectrometry (MS) analysis was performed to screen for differentially expressed proteins. In the Validation Cohort (n = 78), candidate proteins were validated using ELISA in a broader cohort including LCBM patients and those with other neurological conditions (primary intracranial tumors, CNS lymphoma, encephalitis, cerebral hemorrhage, and epilepsy). Finally, prognostic evaluation analyses were performed to evaluate the diagnostic performance (ROC curves) and survival prognosis (Kaplan-Meier curves) of the identified biomarkers for LCBM.

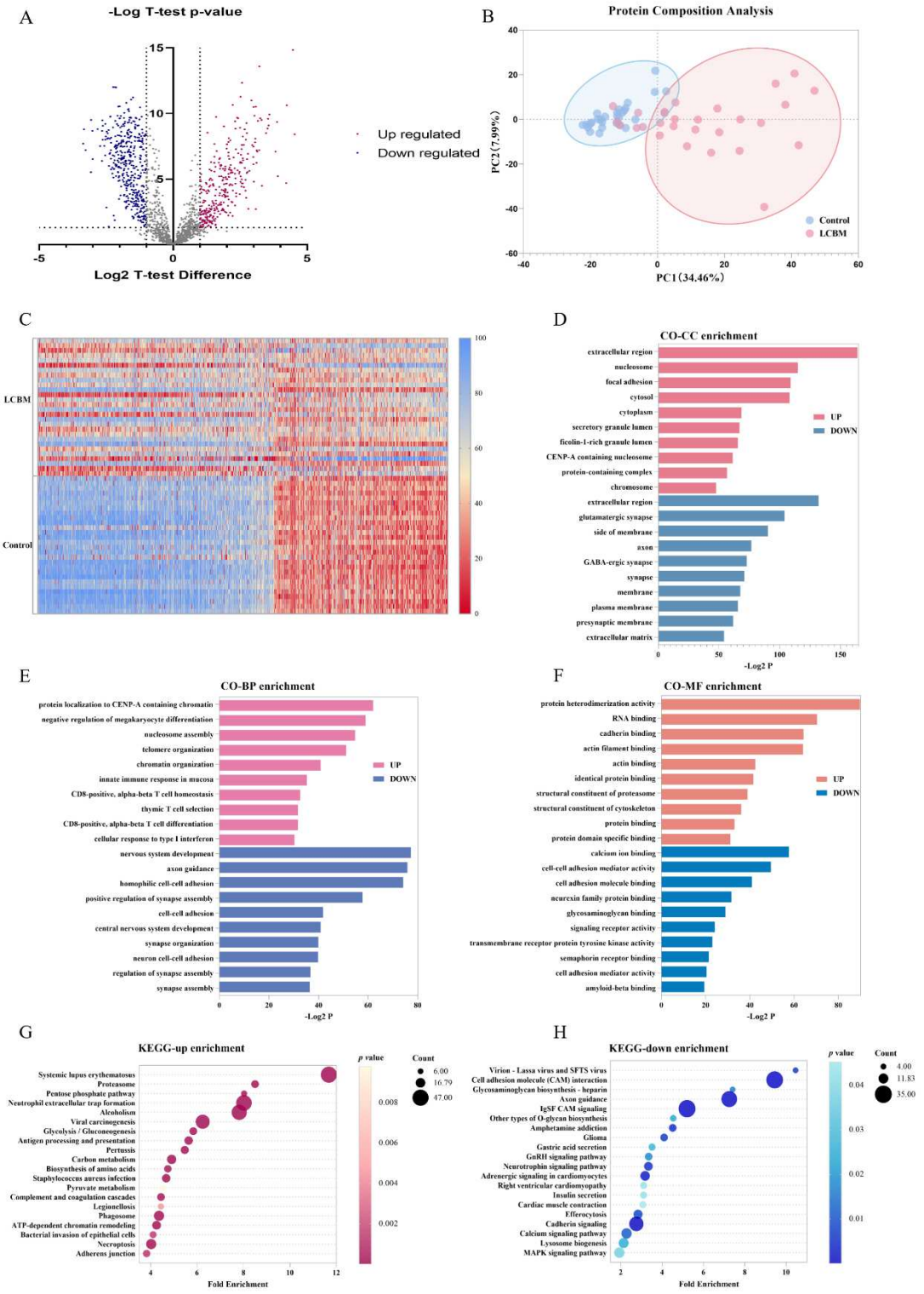


Figure 2. Characterization and functional enrichment analysis of the CSF proteome in the discovery cohort.

The discovery cohort included a total of 56 subjects, consisting of 28 patients with LCBM and 28 controls (patients undergoing lumbar anesthesia for joint surgery).

(A) Volcano plot displaying the results of mass spectrometry-based proteomic analysis of CSF samples. The dashed line represents the significance threshold ($p < 0.05$, corresponding to -log10 $p = 1.301$). Red dots indicate proteins significantly upregulated in the LCBM group, while blue dots indicate significantly downregulated proteins.

(B) Principal component analysis (PCA) plot of the CSF proteome. Sample clustering reveals distinct grouping trends, with the blue area corresponding primarily to control samples and the pink area to LCBM samples.

(C) Heatmap of DEPs, visually demonstrating the divergence in protein expression profiles between the LCBM and control groups.

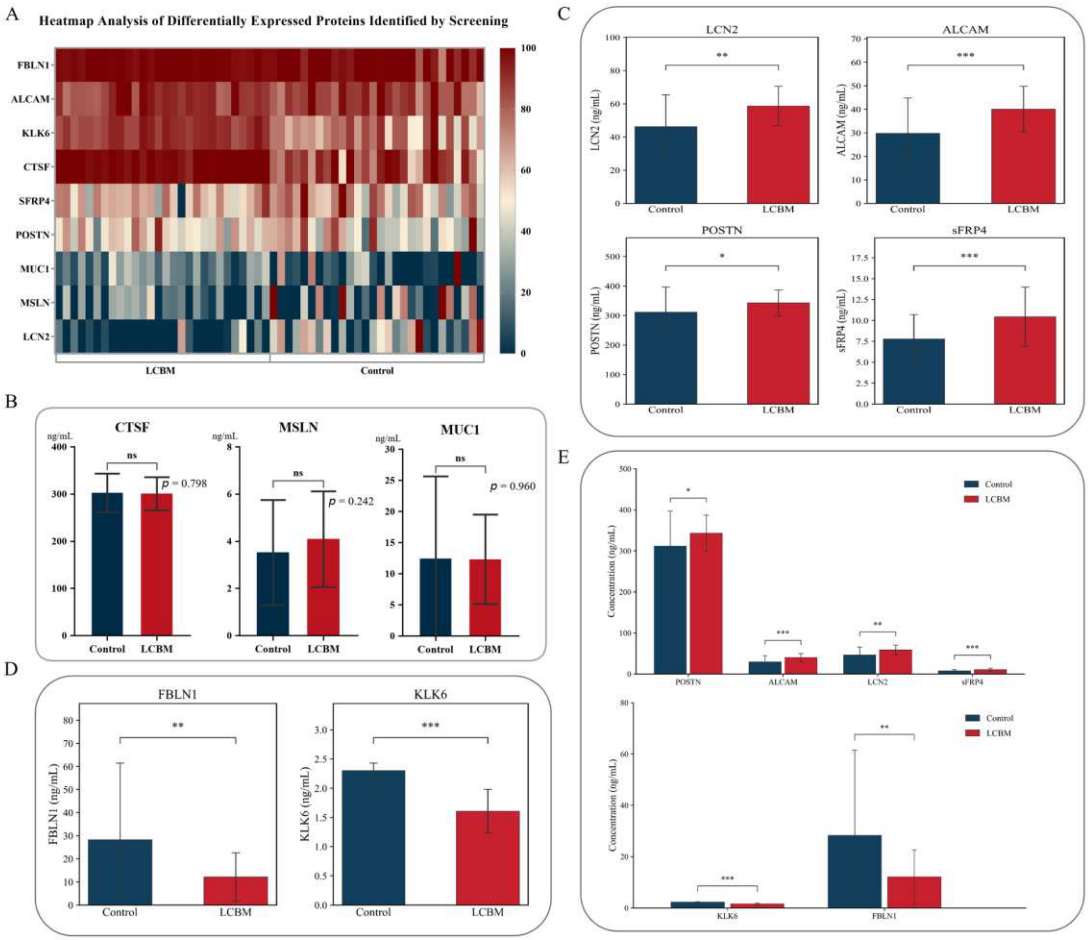
(D) Gene Ontology (GO) enrichment analysis of DEPs (top 10 entries ranked by p value). Cellular Component (CC);

(E) Biological Process (BP);

(F) Molecular Function (MF).

(G) Kyoto Encyclopedia of Genes and Genomes (KEGG) pathway enrichment analysis of DEPs (ranked by Fold Enrichment, top 20 pathways shown). Enriched pathways for upregulated proteins;

(H) Enriched pathways for downregulated proteins.



977

978 **Figure 3. Validation of candidate biomarker levels in the CSF of the validation cohort**
979 **using ELISA.**

980 The validation cohort comprised 78 subjects, including 38 patients with LCBM and 40 controls.
981 The control group consisted of 11 patients with primary intracranial tumors, 5 with central nervous
982 system involvement of lymphoma, 6 with encephalitis, 12 with cerebral hemorrhage, and 6 with
983 epilepsy.

984 (A) Heatmap of the 9 target proteins selected based on pathway analysis of differentially expressed
985 proteins and literature review.
986 (B) ELISA validation of the 9 target proteins. No statistically significant differences were observed
987 for CTSF, MSLN, and MUC1 between the experimental and control groups.
988 (C) Expression levels of POSTN, ALCAM, LCN2, and sFRP4 were significantly upregulated in the
989 experimental group.
990 (D) Expression levels of FBLN1 and KLK6 were significantly downregulated in the LCBM group.
991 (E) Summary of the significantly upregulated and downregulated differentially expressed proteins
992 in the experimental group.

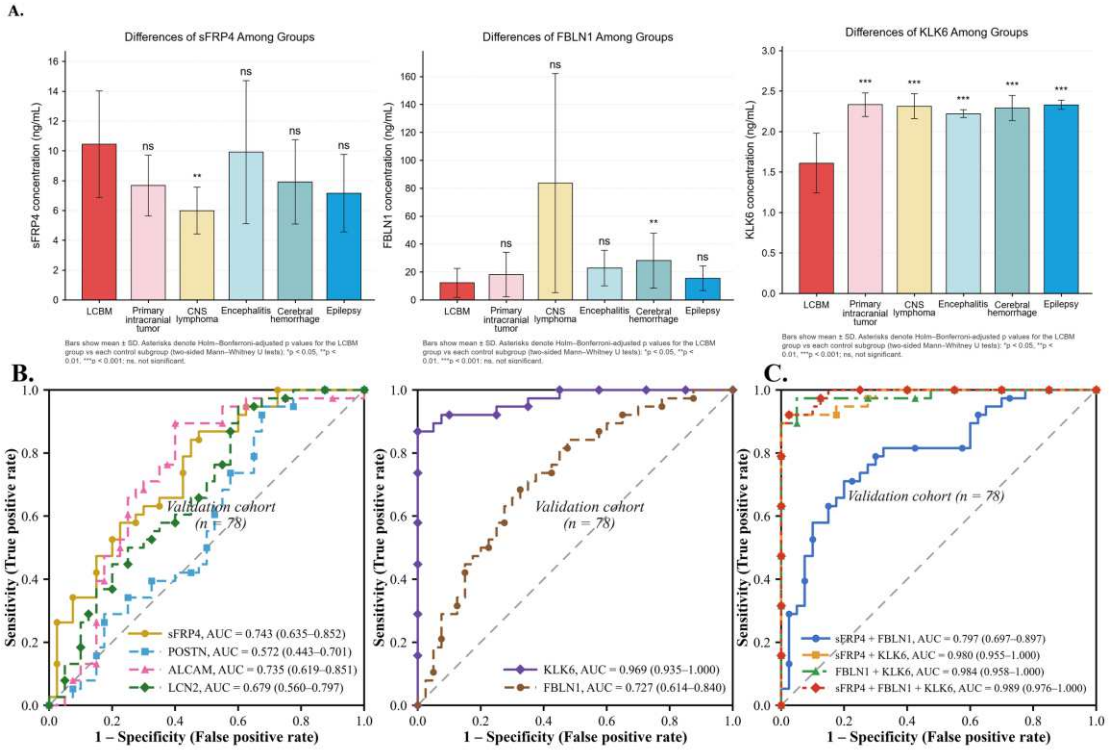


Figure 4. Diagnostic performance evaluation of the identified biomarkers.

(A) Intergroup comparative analysis of the ELISA-validated proteins sFRP4, FBLN1, and KLK6 in the validation cohort (n = 78). Bars show mean ± SD; asterisks denote Holm–Bonferroni-adjusted *p* values for two-sided Mann–Whitney U tests comparing the LCBM group with each disease-control subgroup (*$p < 0.05$, **$p < 0.01$, ***$p < 0.001$; ns, not significant). KLK6 exhibited the most pronounced and consistent intergroup separation, being significantly lower in LCBM than in all five control subgroups (all adjusted $p \leq 0.001$).

(B) ROC curve analysis of the upregulated (left) and downregulated (right) proteins in the validation cohort (n = 78). Among the upregulated proteins, sFRP4 demonstrated the highest diagnostic efficacy (AUC = 0.743); among the downregulated proteins, KLK6 achieved near-perfect discrimination (AUC = 0.969), while FBLN1 yielded an AUC of 0.727.

(C) Construction and evaluation of combined logistic regression diagnostic models in the validation cohort (n = 78). All models incorporating KLK6 achieved near-perfect discrimination (AUC 0.980–0.989), whereas the sFRP4 + FBLN1 combination yielded an AUC of 0.797 (bootstrap-corrected AUC = 0.791). Because KLK6 almost completely separated the two groups in this cohort, the ternary model (sFRP4 + FBLN1 + KLK6) should be regarded as preliminary pending independent external validation.

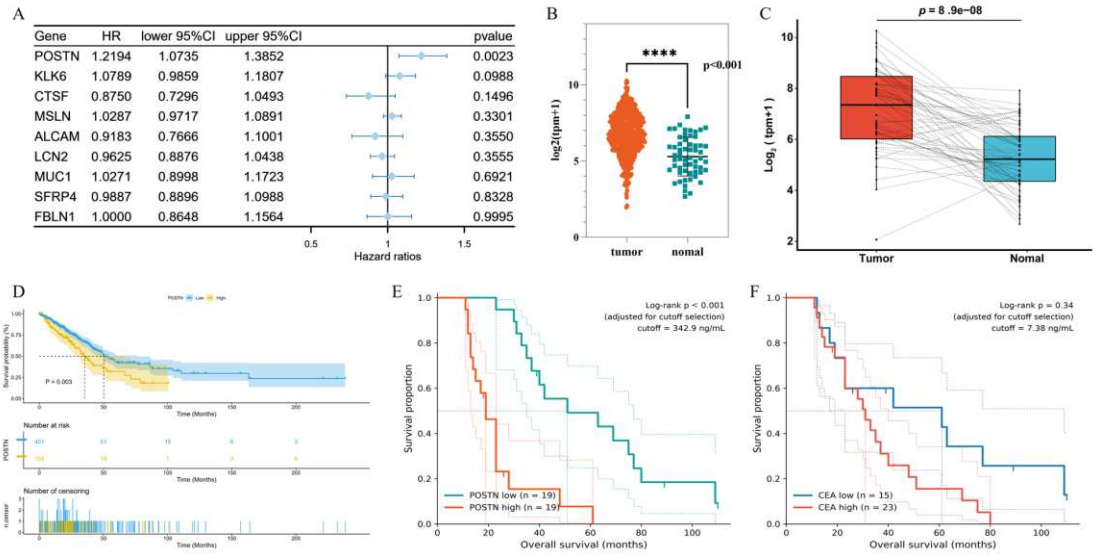


Figure 5. Prognostic value of POSTN in patients with LCBM.

(A) Forest plot displaying the hazard ratios (HR) for overall survival associated with differentially expressed proteins based on TCGA database analysis. POSTN exhibited the most significant prognostic value among the candidates ($p = 0.0023$).

(B) Comparison of POSTN mRNA expression levels between lung cancer tissues and normal tissues (unpaired) using TCGA data. Significantly higher expression was observed in tumor samples ($p < 0.0001$).

(C) Paired analysis of POSTN expression in lung cancer tissues versus adjacent normal tissues from the TCGA database, confirming significant upregulation in tumors ($p = 8.9\times10^{-8}$).

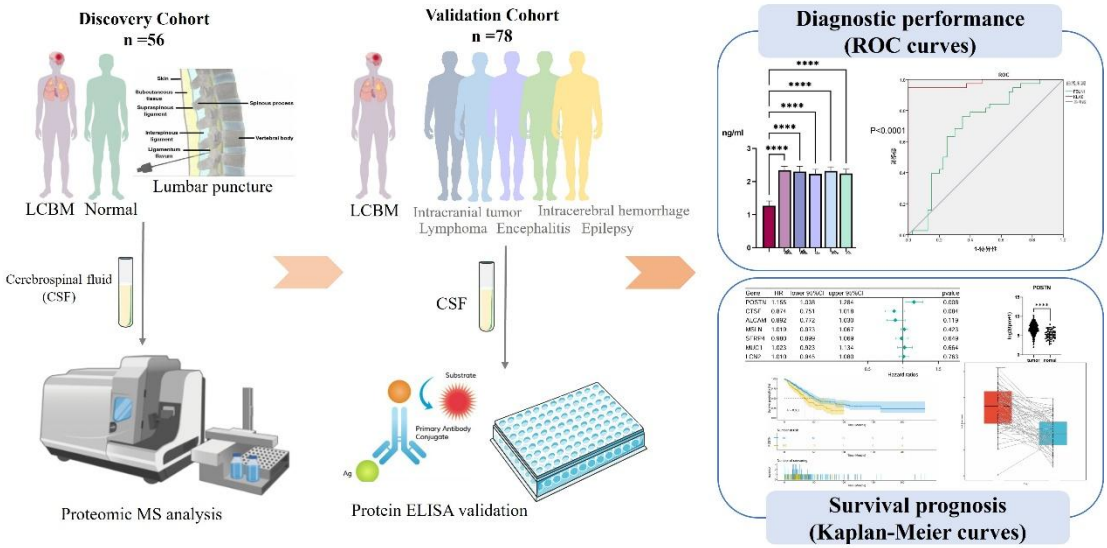
(D) Kaplan-Meier survival curves stratified by POSTN expression levels in the TCGA cohort. Patients with high POSTN expression showed significantly poorer overall survival compared to those with low expression ($p = 0.003$). These TCGA analyses reflect POSTN mRNA in primary lung tumor tissue from unselected patients and are presented as biological context rather than validation of CSF POSTN in LCBM.

(E) Kaplan–Meier analysis of overall survival in LCBM patients stratified by CSF POSTN. Patients were dichotomized at the data-driven optimal cutoff of 342.9 ng/mL determined by maximally selected rank statistics (POSTN high, n = 19; POSTN low, n = 19). Dashed lines indicate 95% confidence bands; vertical ticks denote censored observations. Patients with high CSF POSTN had significantly shorter overall survival than those with low POSTN (median OS, 19.0 vs. 51.0 months; nominal log-rank $p < 0.001$; *$p < 0.001$ after adjustment for cutoff selection by permutation testing*; Cox HR = 6.13 for POSTN-high vs. POSTN-low, 95% CI 2.59–14.49, $p < 0.001$).

(F) Kaplan–Meier analysis of overall survival in LCBM patients stratified by CSF CEA. Patients were dichotomized at the data-driven optimal cutoff of 7.38 ng/mL determined by maximally selected rank statistics, with a minimum proportion of 20% required in each group (CEA high,

n = 23; CEA low, n = 15). Dashed lines indicate 95% confidence bands; vertical ticks denote censored observations. High CEA levels showed a trend toward poorer prognosis that did not reach statistical significance (median OS, 31.0 vs. 61.0 months; nominal log-rank p = 0.055; p = 0.34 after adjustment for cutoff selection by permutation testing; dichotomized Cox HR = 2.08 for high vs. low, 95% CI 0.96–4.52, p = 0.064); in continuous Cox analysis, log-CEA was likewise not significant (HR = 1.26 per SD, 95% CI 0.91–1.75, p = 0.165). This exploratory analysis requires validation in an independent cohort.

Data are presented as mean ± SD or median with interquartile range where applicable. Statistical significance was determined using the log-rank test for survival analysis and t-tests/Wilcoxon tests for expression comparisons.



1047

1048 **TOC**

Supplementary Files

This is a list of supplementary files associated with this preprint. Click to download.

- SupplementaryFigure1.Proteinscreeningflowchart.docx
- SupplementaryFigure2.Calibrationcurves.docx
- SupplementaryTable1.Ageadjustedsensitivityanalysisofthediscoverycohortproteomicscreen.docx
- SupplementaryTable2.Participantcharacteristicsofthediscoveryandvalidationcohorts.docx
- SupplementaryTable3.Differentialproteinexpressioninthediscoverycohort1674proteinscompletestatistics.docx
- SupplementaryTable4.ScreeningofdownregulatedCSFproteinsasELISAvalidationtargets.docx
- SupplementaryTable5.ScreeningofupregulatedCSFproteinsasELISAvalidationtargets.docx
- SupplementaryTable6.Centredistributionandcentrestratifiedsensitivityanalyses.docx
- SupplementaryTable7.PosthoccomparisonsoftheLCBMgroupwitheachcontrolsubgroup.docx
- SupplementaryTable8.PerpatientCSFconcentrationsoftheninecandidateproteinsinthevalidationcohort.docx
- SupplementaryTable9.Coefficientsofthecombinedridgelogisticregressionmodelsandinternalvalidationoftheindividualandcombineddiagnosticmodels.docx
- SupplementaryTable10.CoxanalysesofCSFPOSTNandoverallsurvivalandformalcomparisonofprognosticdiscriminationofCSFPOSTNvsCSFCEA.docx